ELSEVIER

Coastal Engineering 46 (2002) 175–211

Coastal Engineering
An International Journal for Coastal, Harbour and Offshore Engineers

www.elsevier.com/locate/coastaleng

Temporal and spatial variations of surf-zone currents and suspended sediment concentration

Ping Wang [a,*], Bruce A. Ebersole [b], Ernest R. Smith [b], Bradley D. Johnson [b]

[a] *Department of Geology, University of South Florida, 4202 East Folwer Avenue, SCA 528 Tampa, FL 33620, USA*
[b] *U.S. Army Engineer Research and Development Center, Coastal and Hydraulic Laboratory, 3909 Halls Ferry Road, Vicksburg, MS 39180, USA*

Received 16 November 2001; received in revised form 22 May 2002; accepted 14 June 2002

Abstract

Temporal and spatial variations of surf-zone currents and suspended sediment concentrations were investigated at the U.S. Army Engineer Research and Development Center's Large-scale Sediment Transport Facility (LSTF). A longshore-uniform fine-sand beach, 35 m alongshore, 20 m cross-shore, and 25 cm thick was placed in the facility for these experiments. Two unidirectional, long-crested irregular wave conditions were examined, one resulted in predominantly spilling breakers and one in plunging breakers. Waves and currents, and sediment concentrations were measured at 20 and 16 Hz, respectively, at various longshore and cross-shore locations and throughout the water column. Both currents and sediment concentrations exhibit great temporal and spatial variations in the surf zone. The variation patterns, however, of the longshore current, cross-shore current, and sediment concentration are substantially different. Caution should be exercised when averaging these parameters over time and space.

For the two wave cases examined, the temporal variations of longshore current, including those at principal incident-wave frequencies, were relatively small across most of the surf zone. Over 70% of the variations are within approximately $\pm 60\%$ of the mean value. The wave motion, with a strong peak at principal incident-wave frequencies, dominated the temporal variations of cross-shore current. Temporal variations of suspended sediment concentration under the irregular waves were episodic, characterized by occasional large values induced by suspension events or due to horizontal advection. The variance of the concentration at the peak incident-wave frequency was not significant except very near the bed.

Time-averaged longshore-current profiles over the predominantly rippled sand bed were logarithmic in shape below the wave trough. Depth-averaged longshore current (excluding the portion of water column above wave trough) matched well with the current measured at an elevation of 1/3 of the water depth from the bed. Time-averaged cross-shore current profiles were characterized by an onshore mass flux near the surface, and a balancing offshore flow below the wave-trough level (undertow). Sediment concentration decreased very rapidly upward through the water column across most of the surf zone except at the plunging breaker line where relatively homogeneous concentration was measured throughout much of the water column above 4 cm from the bed. Depth-averaged sediment concentration over the range from 1 cm above the bed to the bottom of wave trough roughly equaled the concentration measured at an elevation from the bed equal to 20% of the still-water depth.

* Corresponding author. Tel.: +1-813-974-9170; fax: +1-813-974-2654.
E-mail address: pwang@chuma1.cas.usf.edu (P. Wang).

PII: S0378-3839(02)00091-1

A reasonable estimate of the time-averaged longshore sediment flux was obtained from the product of time-averaged profiles of longshore current and sediment concentration. Accurate estimates of time-averaged cross-shore sediment flux, however, could not be obtained from the product of time-averaged current and concentration.

Keywords: Surf-zone sediment transport; Surf-zone hydrodynamics; Sediment suspension; Longshore sediment transport; Cross-shore sediment transport; Physical modeling; Sediment flux

1. Introduction

Sediment concentration along with fluid velocity determines sediment flux. A general form for computing sediment flux is given as

$$F_{x,y}(x,y,z,t) = u_{x,y}(x,y,z,t) \times c(x,y,z,t) \quad (1)$$

where F is sediment flux per unit area; u is current velocity; c is sediment concentration; t is time; and x, y, and z are cross-shore, longshore, and vertical coordinates, respectively. $u_{x,y}$ denotes u_x or u_y, which represents cross-shore or longshore current, respectively. Variations in the longshore direction are typically much less than those in the cross-shore and vertical directions and are, therefore, often neglected, reducing Eq. (1) to

$$F_{x,y}(x,z,t) = u_{x,y}(x,z,t) \times c(x,z,t) \quad (2)$$

Due to the dynamic nature of the surf zone, simultaneously determining the fluid velocity and sediment concentration with adequate temporal and spatial resolutions is difficult. Less detailed approaches, typically empirical ones, are commonly used to determine a temporally averaged and spatially integrated sediment transport rate. For example, the broadly used CERC formula assumes that the total rate of longshore sediment transport in the surf zone is proportional to longshore energy flux at the main breaker line (USACE, 1984; Wang et al., 1998). No temporal scale is specified in the CERC formula and the spatial scale spans the entire surf zone. The cross-shore sediment transport rate per unit width of beach is often determined from time-varying beach profile changes with temporal scales of up to months or even years (Dean, 1977; Dean and Zheng, 1994; Zheng and Dean, 1997).

In order to examine the influences of the complicated temporal variations and phase coupling of the surf-zone current and sediment concentration for the determination of sediment flux, $u_{x,y}$ and c are often partitioned as (e.g., Osborne and Greenwood, 1993; Grasmeijer and Van Rijn, 1999; Thornton et al., 1996)

$$u_{x,y} = \bar{u}_{x,y} + \tilde{u}_{x,y\_\mathrm{low}} + \tilde{u}_{x,y\_\mathrm{high}} \quad (3)$$

$$c = \bar{c} + \tilde{c}_{\mathrm{low}} + \tilde{c}_{\mathrm{high}} \quad (4)$$

where $\bar{u}$ and $\bar{c}$ are the time-averaged velocity and sediment concentration, respectively. $\tilde{u}$ and $\tilde{c}$ are oscillatory components of velocity and concentration. The subscripts *high* and *low* indicate high (e.g., wind wave) and low (e.g., infragravity) frequency components. The time-averaged sediment flux is then determined as

$$\overline{F_{x,y}} = \overline{u_{x,y}c} = \bar{u}_{x,y}\bar{c} + \overline{\tilde{u}_{x,y\_\mathrm{low}}\tilde{c}_{\mathrm{low}}} + \overline{\tilde{u}_{x,y\_\mathrm{high}}\tilde{c}_{\mathrm{high}}} \quad (5)$$

The second and third terms on the right-hand side are poorly understood and often neglected or simplified in sediment transport modeling. An improved understanding of the temporal variations of surf-zone hydrodynamics and sediment concentration is essential to improve our capability of predicting sediment flux. To obtain a transport rate across an area of interest, e.g., longshore transport rate across the surf zone, it is necessary to integrate the point sediment flux (Eq. (5)) over space, which requires knowledge of spatial variation. One of the goals of this paper is to document the temporal and spatial variations of surf-zone current and sediment concentration over a large laboratory beach.

The analyses presented here are based on data collected in the recently established Large-scale Sediment Transport Facility, LSTF (Hamilton et al., 2001; Hamilton and Ebersole, 2001; Wang et al., 2002; Wang and Kraus, in press). Two unidirectional long-crested irregular wave conditions, with one resulting in pre-

dominantly spilling breakers and one in plunging breakers over a fine-sand beach, were investigated. Alongshore and cross-shore distribution patterns of current and sediment concentration were measured. Vertical profiles of fluid velocity and sediment concentration were also measured through the water column at frequencies of 20 and 16 Hz, respectively, allowing the examination of temporal variations due to wave motion.

The objectives of this paper are (1) to examine temporal and spatial variations of surf-zone currents and suspended sediment concentration, (2) to estimate the uncertainties associated with temporal and spatial averaging of the above parameters, (3) to investigate the uncertainties involved in the calculation of sediment flux using temporally and spatially averaged current and concentration, and (4) to compare differences in concentration and sediment flux between predominantly spilling- and plunging-type breakers.

2. The large-scale sediment transport facility (LSTF)

Detailed description of the LSTF is presented in Hamilton et al. (2001). The LSTF has dimensions of 30-m cross-shore, 50-m longshore and has walls 1.4 m high (Fig. 1). The unidirectional, long-crested irregular waves were produced by four synchronized wave generators oriented at a 10° angle to the shoreline. The beach was arranged in a trapezoidal plan shape corresponding to the obliquely incident waves (Fig. 1). The beach is composed of approximately 150 m^3 of very well-sorted fine quartz sand with a median grain size of 0.15 mm and a settling speed of 1.8 cm/s, calculated based on Hallermeier (1981). The sand beach was approximately 25 cm thick, placed over a planar concrete base and extended 27 m alongshore and 18 m cross-shore. Fifteen meters of the beach was below the still-water level and the remaining 3 m was above. The constructed topographic contours were reasonably straight and parallel with the shoreline. The longshore current generated by the obliquely incident waves was circulated with 20 pumps through dedicated flow channels from the downdrift end to the updrift end (Hamilton and Ebersole, 2001). The influences of the lateral boundaries can be minimized by properly circulating the wave-generated longshore current. The present studies focus on the middle section of the test beach, where longshore uniformity in hydrodynamics and morphodynamics was approximated well.

The LSTF hosts a suite of instrumentation (Table 1). Depth-integrated longshore sediment flux was

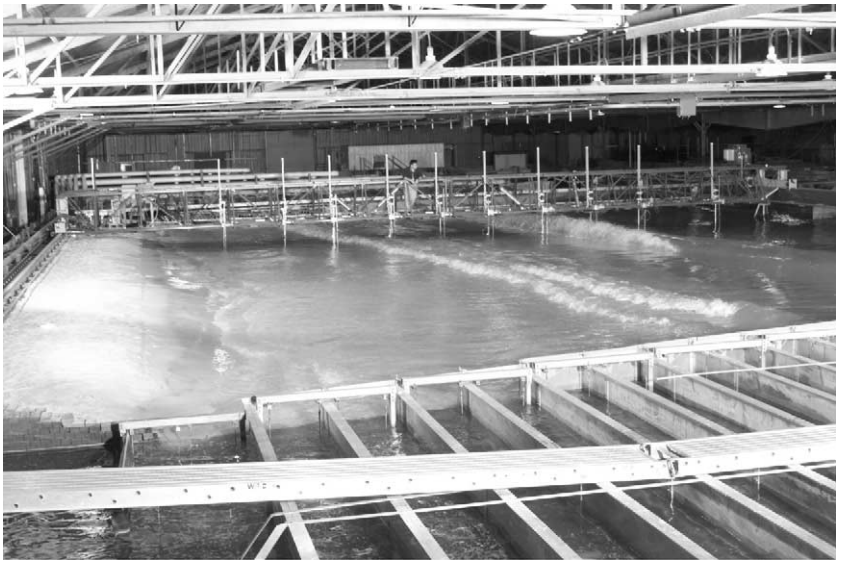

Fig. 1. The LSTF during the plunging case, showing the flow channels (bottom) and the instrument bridge (top) carrying the current meters and wave gages (vertical rods).

Table 1
LSTF instrumentation and the sampling scheme for this study

Parameter to be measured	Instrument type	Sampling rate	Sampling duration	Number of cross-shore locations	Vertical profile
Wave	capacitance gage	20 Hz	10 min	10[a]	N/A
Current	Acoustic Doppler Velocimeter (ADV)	20 Hz	10 min	10	Yes
Sediment concentration	Fiber Optical Backscatter (FOBS)	16 Hz	10 min	7	Yes
Water depth	bottom-tracking profiler	every 5 mm cross-shore	continuous	3660	N/A

[a] The 10 locations were 1.1 m (ADV1), 2.7 m (ADV2), 4.1 m (ADV3), 5.7 m (ADV4), 7.1 m (ADV5), 8.5 m (ADV6), 10.1 m (ADV7), 11.6 m (ADV8), 13.1 m (ADV9), 15.6 m (ADV10) seaward from the still-water shoreline.

measured at twenty 0.75-m-wide downdrift bottom traps, providing data on the cross-shore distribution of longshore sediment transport. The free surface position was measured using capacitance wave gages sampled at a frequency of 20 Hz. Acoustic Doppler Velocimeters (ADVs) were used to measure current (Kraus et al., 1994). The wave and current sensors were colocated at 10 cross-shore locations and synchronized in time (see Table 1 for cross-shore sensor locations). Vertical profiles of velocity were measured by positioning the ADVs at different elevations in the water column at the same alongshore location during a series of wave runs (Hamilton and Ebersole, 2001). Therefore, there were time lags of approximately 15 min (10 min sampling and 5 min for positioning sensors) between velocity measurements at different elevations. Given the constant input wave conditions and negligible beach changes during the series of wave runs, time lags should not have significant influences on data relevancy. Hamilton and Ebersole (2001) and Hamilton et al. (2001) discussed the steadiness in hydrodynamic conditions and measurement repeatability and their implications on making measurements of the vertical structure of velocity.

Profiles of sediment concentration were measured using four arrays of Fiber Optical Backscatter Sensors (FOBS). Each sensor of the array has a vertical resolution of 0.5 cm (Beach et al., 1992) and was calibrated using the sand from the test beach. Elevations of the sensors were controlled by referring them to the bottom one, which was deployed directly on the bed. Each array contains 19 sensors positioned at 0, 1, 2, 3, 4, 5, 6, 7, 9, 11, 13, 15, 17, 21, 27, 33, 39, 45, and 51 cm from the bed. The near-bottom sensors have a smaller spacing of 1 cm as compared to the spacing of 4 to 6 cm for sensors higher in the water column. The FOBS were sampled at 16 Hz and were operated through a separate computer independent of the wave and current sampling system. Due to different lengths of startup time and limitations in the present data acquisition system, the sampling of wave and current data was approximately 3 s behind that of sediment concentration data.

The wave, current, and sediment concentration sensors were mounted on a steel bridge spanning the basin in the cross-shore direction (Fig. 1). This instrument bridge can be moved precisely alongshore, with an accuracy of ± 2 mm. By stationing the bridge at different locations, cross-shore transects of wave, current, and concentration measurements can be conducted at various longshore locations. The bridge also provides a platform for conducting dye experiments and beach-profile surveying. Beach profiles were surveyed using an automated bottom-tracking profiler that travels along the bridge. For the present experiments, the alongshore interval between adjacent beach profiles was 1.0 m (0.5 m near the updrift and downdrift boundaries) and the profiler was programmed to sample every 0.5 cm in the cross-shore direction. Experimental procedures similar to those described in Wang et al. (2002) were followed in this study.

Spectral analyses of water level, current, and sediment concentration data were based on the Welch method (Welch, 1967). The 10-min wave and current records, which were sampled at 20 Hz, were segmented into 1.71-min segments (2048 data points) with 50% overlap. For the 16-Hz sediment-concentration record, the 2048-point segment represented 2.13 min. A confidence interval of 95% was used. A low cutoff at twice the generated peak wave period, i.e., 3 s for the spilling case and 6 s for the plunging case, was applied during the calculation of significant wave height (H_{mo}). This low cutoff had considerable

influence on the determination of H_{mo} at the two landwardmost wave gages within 3 m from the still-water shoreline, where low frequency motions were substantial. Its influences at other cross-shore locations were minimal.

3. Wave and beach conditions

3.1. The input wave conditions

Two unidirectional, long-crested irregular wave conditions, each characterized by a relatively broad spectral shape, were generated based on the TMA spectra (Bouws et al., 1985) with the spectral width parameter of 3.3. Wave condition 1 with greater steepness resulted in predominantly spilling breakers, while wave condition 2 with relatively low steepness resulted in predominantly plunging breakers. Deep-water wave parameters were calculated from the conditions at the wave generator based on linear wave theory. Wave conditions, including both measured and calculated ones, are summarized in Table 2. The main breaker angle was estimated visually using the angle-measuring device in an electronic total survey station. The breaker angles listed represent the averages of over 40 measurements.

The main breaker line was located at about 13.1 m from the shoreline (gage 9, second from offshore) for the spilling case (Fig. 2). For the plunging case, the main breaker line was located at 11.6 m (gage 8, third from offshore). Determination of the main breaker line for irregular waves, and therefore the breaker height, was somewhat subjective. In the present study, the main breaker line was determined to be at the location landward of which a significantly increased gradient of wave-height decay was noticed (Fig. 2). This criterion was based on the comprehension that a drastic wave-energy loss, and therefore wave-height decrease, should follow major wave breaking. Visual observations of "white water" during the wave runs supported the above measure. Similar breaker heights of 0.26 and 0.27 m were measured for the spilling and the plunging cases, respectively. The accuracy of the wave gages was ± 2 mm (Hamilton et al., 2001).

The ratio of significant wave height to water depth ranged mostly from 0.6 to 0.8 (Fig. 2). A greater value of nearly 1 was measured at the plunging breaker line, followed by a sharp decline to slightly less than 0.6. A trend of landward increase of the H_{mo}/h ratio, from slightly below 0.6 to nearly 0.8, was measured across most of the surf zone for both the plunging and the spilling cases, indicating that the rate of wave-height decay was slower than the rate of water-depth decrease in the surf zone. Similar trend was reported by Johnson and Kobayashi (2000). Across the mid-surf zone, which was dominated by surf bores, the magnitudes and trends of significant wave heights and the H_{mo}/h ratio were similar for both the plunging and the spilling cases, while conditions in the vicinities of the breaker line and shoreline were different (Fig. 2).

The spectral density of the free surface fluctuations shows that peak wave period for the spilling and the

Table 2
Summary of the wave and surf-zone conditions

	Spilling breaker case	Plunging breaker case
Conditions at the wave generator (designed)		
Water depth (m)	0.9	0.9
Significant wave height (m)	0.25	0.23
Peak wave period (s)	1.5	3.0
Wavelength (m)	3.4	8.7
Wave celerity (m/s)	2.2	2.9
Wave angle (°)	10	10
Deep-water wave conditions (calculated)		
Significant wave height (m)	0.27	0.24
Peak wave period (s)	1.5	3.0
Wavelength (m)	3.5	14.0
Wave celerity (m/s)	2.3	4.7
Wave angle (°)	10.4	16.3
Wave steepness	0.077	0.017
Breaking wave conditions (measured)		
Significant breaker height (m)	0.26	0.27
Main breaker angle (°)	6.5	6.4
Breaking water depth (m)	0.46	0.28
Breaker index (H_{mo}/h)	0.57	0.96
Surf zone conditions (measured)		
Surf zone width[a] (m)	14.0	13.0
Surf zone slope[b]	1:28 (0.035)	1:43 (0.023)

[a] The surf zone width also includes the uprush zone above the still-water shoreline.

[b] The overall surf zone slope is calculated as the plane slope from the breaker point to the still-water shoreline.

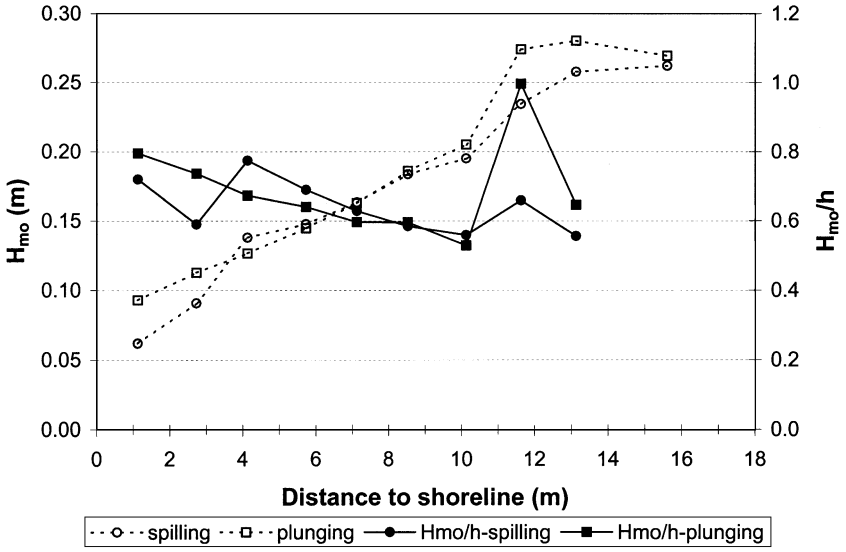

Fig. 2. Cross-shore distribution of significant wave height and breaker index defined as H_{mo}/h.

plunging cases is 1.5 s (0.67 Hz) and 3.0 s (0.33 Hz), respectively, with various amounts of low frequency energy (Fig. 3). The period of the low-frequency peak varied somewhat across the surf zone but remained mostly between 11 s (0.09 Hz) and 21 s (0.05 Hz). Its relative energy density increased substantially toward shore, becoming the dominant peak at the two landwardmost gages, 1.1 and 2.7 m from the shoreline, respectively. Low-frequency motion was found to have significant influence on sediment transport in the swash zone and immediately seaward (e.g., Puelo et al., 2000).

3.2. Beach conditions

The test beach was initially constructed based on the equilibrium profile shape described by Bruun (1954) and Dean (1977) in the form of

$$h = Ax^{\frac{2}{3}} \tag{6}$$

where h is still-water depth, x is horizontal distance from the shoreline, A is a dimensional-scaling parameter determined by sediment grain size to be 0.07 $m^{1/3}$ based on the Dean (1991) method. The beach profile calculated using Eq. (6) was approximated with three planar segments for convenience of construction. Approximately 20 min of wave action was imposed before the survey of the initial beach to smooth out the tractor-tire tracks from construction. This wave action caused the slight deviation from the segmented planar beach in the offshore region from 9 to 13 m (Fig. 4).

The spilling case, which lasted a total of 33 h, was conducted with the power-function profile of Eq. (6) as the initial condition. The spilling-breaker experiment was conducted in eighteen 15- to 200-min segments (Wang et al., 2002). The beach profile was surveyed at the end of each segment. The modest change of beach-profile shape (Fig. 4) occurred during the first 22 h. The beach profile reached quasi-equilibrium, or stable shape, after 22 h of the spilling-wave action. The spilling profile shown in Fig. 4 represents the average of 16 profiles in the middle section of the test beach surveyed between 22 and 33 h. Boundary effects in the middle 16 m of the test beach were negligible. Modest erosion was measured in the inner surf zone between 0.5 and 5.0 m from shoreline, while modest accumulation was measured in the vicinity of the breaker line from 9.5 to 14.5 m. Little net change in bed elevation was measured in the mid-surf zone between 5.0 and 9.5 m. The hydrodynamic and sediment concentration data presented here are those collected after equilibrium between 22 and 33 h.

The plunging-breaker case, which lasted a total of 10.5 h, was conducted after the spilling case, using the

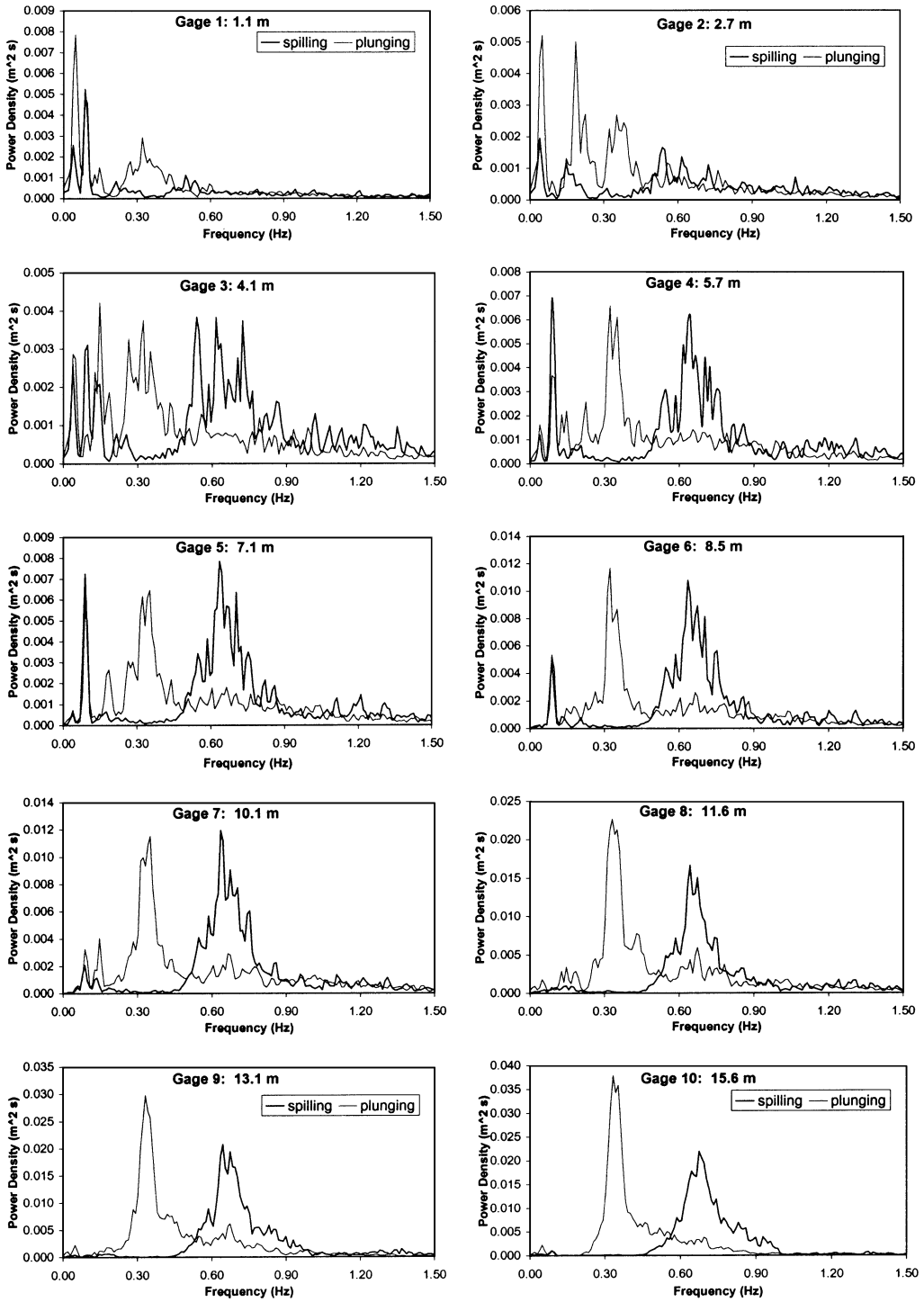

Fig. 3. Spectral characteristics of water-level fluctuations at different cross-shore locations for both spilling and plunging cases.

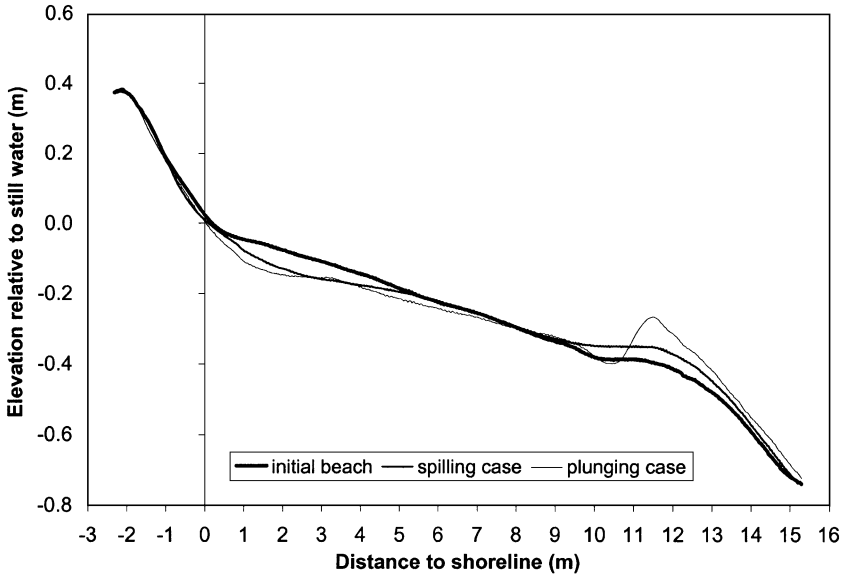

Fig. 4. Initial and equilibrium beach profiles for the two wave cases.

final profile from the spilling waves as the initial profile. The beach profile reached quasi-equilibrium after 6.3 h of the plunging-wave action. The plunging case was conducted in thirteen 40- to 100-min segments. Considerable changes in profile shape were measured for the plunging-breaker case, mainly at the plunging point, where a substantial breakpoint bar developed (Fig. 4). The plunging profile shown in Fig. 4 represents the average of 16 profiles in the middle section of the test beach surveyed between 6.3 and 10.5 h. Less change was observed in other parts of the profile. Only the data collected after the equilibrium between 6.3 and 10.5 h are discussed here. In Fig. 4 and subsequent figures, the x-axis (cross-shore direction) is positive seaward and is referenced to the still-water shoreline of the initially constructed beach, which was designed to be located at 3 m from the basin wall.

Bed ripples developed over the entire surf zone under the spilling breakers except in the vicinity of the shoreline (Fig. 5). Most of the ripples were 0.7 to 1.2 cm high with ripple lengths ranging from 6 to 10 cm (Fig. 5, insert). Under the plunging breakers, ripples formed in the mid-surf zone, while in the vicinities of the breaker line and shoreline, a relatively featureless bed was observed. Most of the ripples were 1.0 to 1.5 cm high with ripple lengths ranging from 8 to 12 cm. Although some variations were observed, particularly seaward of the breaker line, the ripple crests were predominantly parallel to the shoreline.

For the convenience of discussion, the commonly used nearshore zonation is defined as follows. The swash zone ranged from the landward limit of uprush to the seaward extent of the planar bed, which roughly coincides with the seaward limit of the backwash. For the spilling case, the swash zone extended, on average, from -0.9 to 0.5 m. For the plunging case with waves of longer period, the swash zone extended from -1.1 to 0.9 m, about 43% wider than for the spilling case (Fig. 5). The breaker zone, where main wave breaking occurred, ranged from 10 to 13 m for the plunging case and 11 to 14 m for the spilling case. The bar crest was located at about 11.5 m for both cases. The mid-surf zone lies between the swash and the breaker zones and ranged from 0.5 to 11 m for the spilling case and 0.9 to 10 m for the plunging case.

A greater wave setup, 1.3 vs. 1.0 cm, was measured for the longer period waves of the plunging case than for the spilling case (Fig. 6). For the spilling case, maximum setdown of 0.4 cm occurred at 10.1 m from shoreline, slightly landward of the main breaker line identified from the trend of wave-height decay (Fig. 2). For the plunging case, maximum setdown of 0.7 cm occurred at 11.6 m, coinciding with the main

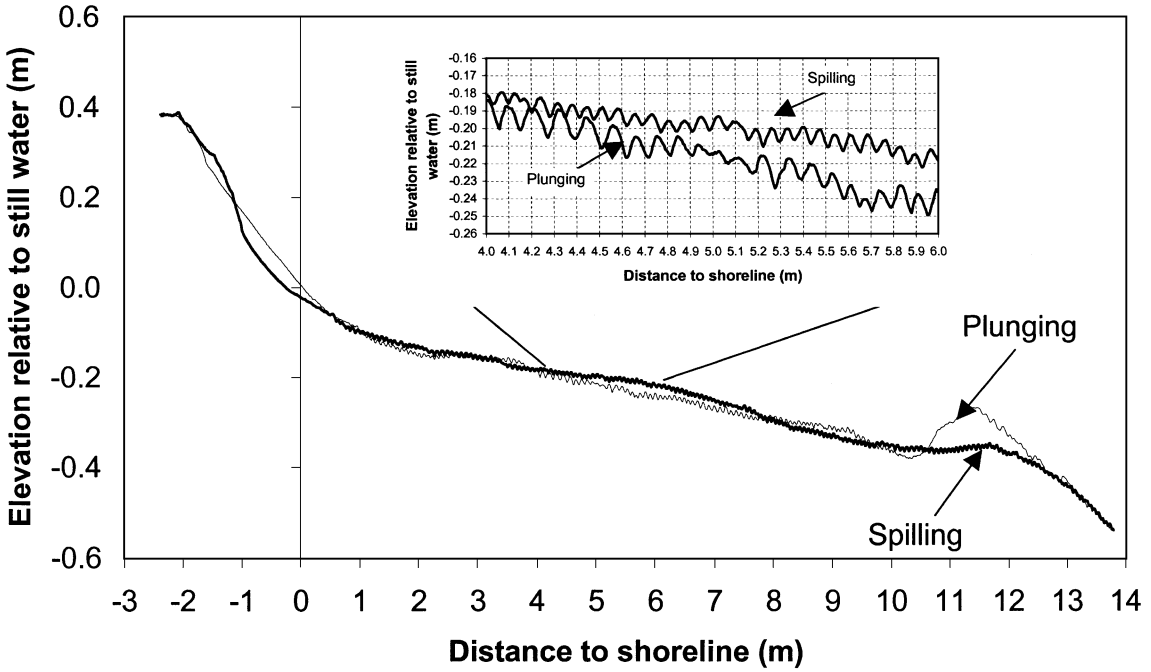

Fig. 5. Examples of beach profile obtained during the spilling and plunging cases. Profiles surveyed in the middle of the test beach at 23 h for spilling and 7.3 h for plunging.

breaker line. Maximum setup was measured at the landwardmost gage, 1.1 m from the shoreline. The data shown in Fig. 6 represent averages of nine and four measurements spanning the middle 16 m of the test beach for spilling and plunging case, respectively. The error bars indicate the ranges of one standard

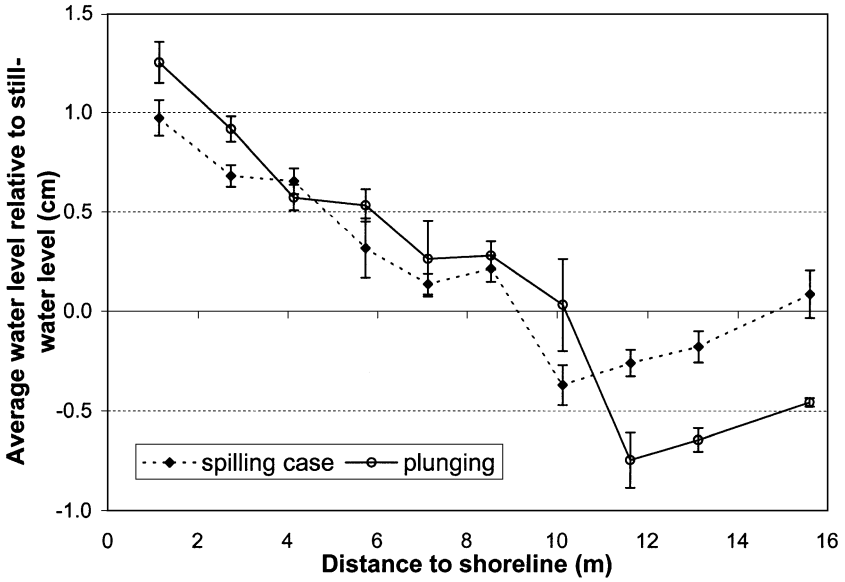

Fig. 6. Setup and setdown during the spilling and plunging cases.

deviation and are included to demonstrate the degree of alongshore variability.

4. Results and discussion

4.1. Temporal variations of surf-zone currents

4.1.1. Temporal variations and periodicities of cross-shore currents

Fig. 7 shows the dimensionless power spectral density for the cross-shore current measured at 1/3 water depth from the bottom for both wave cases. The dimensionless power spectral density was computed as

$$\mathrm{PSD}_{\mathrm{dimensionless}}(i) = \frac{\mathrm{PSD}(i)}{\mathrm{Max}(\mathrm{PSD})} \quad i = 1, 2, 3, \ldots \qquad (7)$$

where PSD(i) is the power spectral density of frequency component i, and Max(PSD) is the peak spectral density. Fig. 7 illustrates the shape of the spectral density instead of the absolute magnitude.

Overall, the spectral shapes are similar to those of water-level fluctuation (Fig. 3), as expected. At most locations, the peak period of the cross-shore current fluctuations was 1.5 s (0.67 Hz) and 3.0 s (0.33 Hz) for the spilling and the plunging cases, respectively, with secondary low-frequency peaks from 11 s (0.09 Hz) to 21 s (0.05 Hz), respectively. The relative spectral density at the low frequency dominates near the shoreline in a pattern similar to the free surface. These similarities are expected because the waves, with a small incident-wave angle of 10°, dominated the cross-shore current. The increase of the low-frequency components toward the shoreline is well documented in both laboratory (e.g., Thompson and Briggs, 1993) and field (e.g., Huntley et al., 1981; Guza and Thornton, 1982).

The two landwardmost ADVs were occasionally exposed to air due to the shallow and varying water depth, resulting in a considerable fraction (approximately 15% to 30%) of erroneous data in the form of unrealistic spikes. These erroneous points were removed during data analysis using the procedure described in Hamilton et al. (2001) and Hamilton and Ebersole (2001). However, because the influences of these spikes, or their removal on spectral analysis are not clear, the two landwardmost ADVs are excluded from the frequency analysis.

4.1.2. Temporal variations and periodicities of longshore currents

Overall, the frequency distribution of longshore current was substantially different from the patterns of the cross-shore current and water-surface fluctuations especially in the surf zone landward of gage 8 (Fig. 8). The peak spectral density usually occurred at a much lower frequency, between 50 and 100 s, than that associated with either the peak incident waves or the 10- to 20-s low-frequency range observed in the cross-shore currents. The 50- to 100-s low-frequency peak was an artifact of the data segmenting and windowing applied in the present power spectral density analysis. No low-frequency cutoff was imposed. Qualitative examination of the raw data did not indicate apparent low-frequency variation having 50- to 100-s period. It is worth noting that Figs. 7 and 8 illustrate the shapes of the spectral density instead of the magnitudes. The magnitudes of the spectral density of the cross-shore current were much greater, typically over one order of magnitude greater, than those of the longshore current.

Across most of the mid-surf zone (gages 3 through 7), the variance of longshore current at the incident-wave frequencies was small. A narrow spectral peak occurred at approximately 1.5 s at ADV6 for the spilling case. The energy carried by this narrow peak was low. This peak is partially related to the small frequency interval used in the spectral analyses with the objective of fine spectral resolution. Secondary peaks occurred between 10 and 20 s for both wave cases, similar to the distributions of cross-shore current and water-level spectral density. Near and seaward of the breaker line (gages 8 through 10), spectral density at the incident-wave frequency became apparent. Although the spectral shapes resemble those of cross-shore current (Figs. 7 and 8), the magnitudes of the longshore current variance were much smaller.

Overall, the temporal variations of longshore current were not significantly influenced by the frequency of the wave-induced orbital motion across most of the surf zone, as indicated by the general lack of the spectral peak at 0.67 Hz (1.5 s) and 0.33 Hz (3.0 s), respectively. Temporal variations of long-

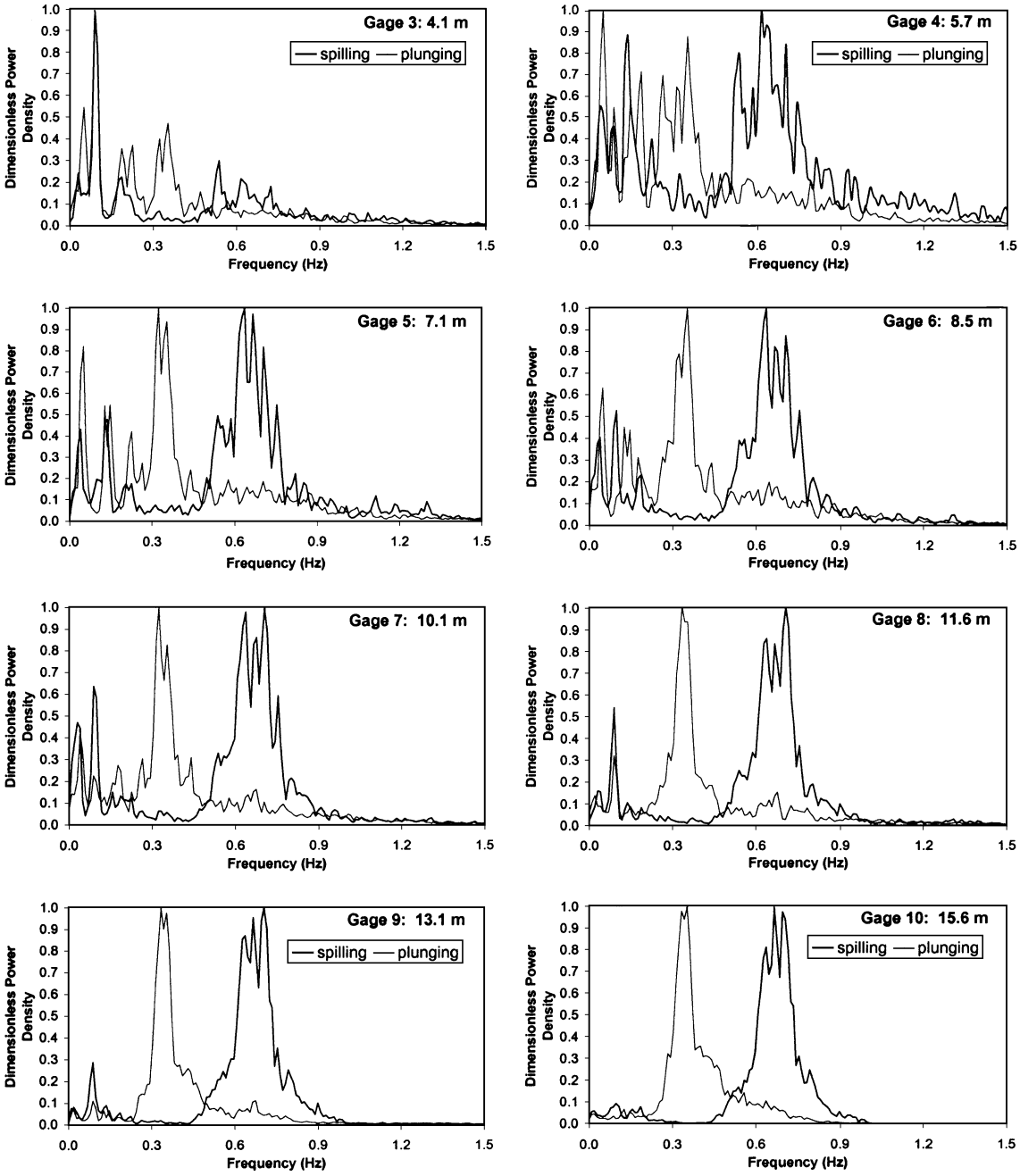

Fig. 7. Spectra of the temporal variations of cross-shore current.

shore current were relatively small in magnitude, compared to the mean value (Fig. 9). The temporal variation, as indicated by one standard deviation, was 44% of the mean value for the spilling case examples (top two panels). Examples from two elevations (1/3 and 2/3 of the still-water water depth from the bottom) at ADV6 location (8.5 m from shoreline), a short distance landward of the breaker line, are illustrated.

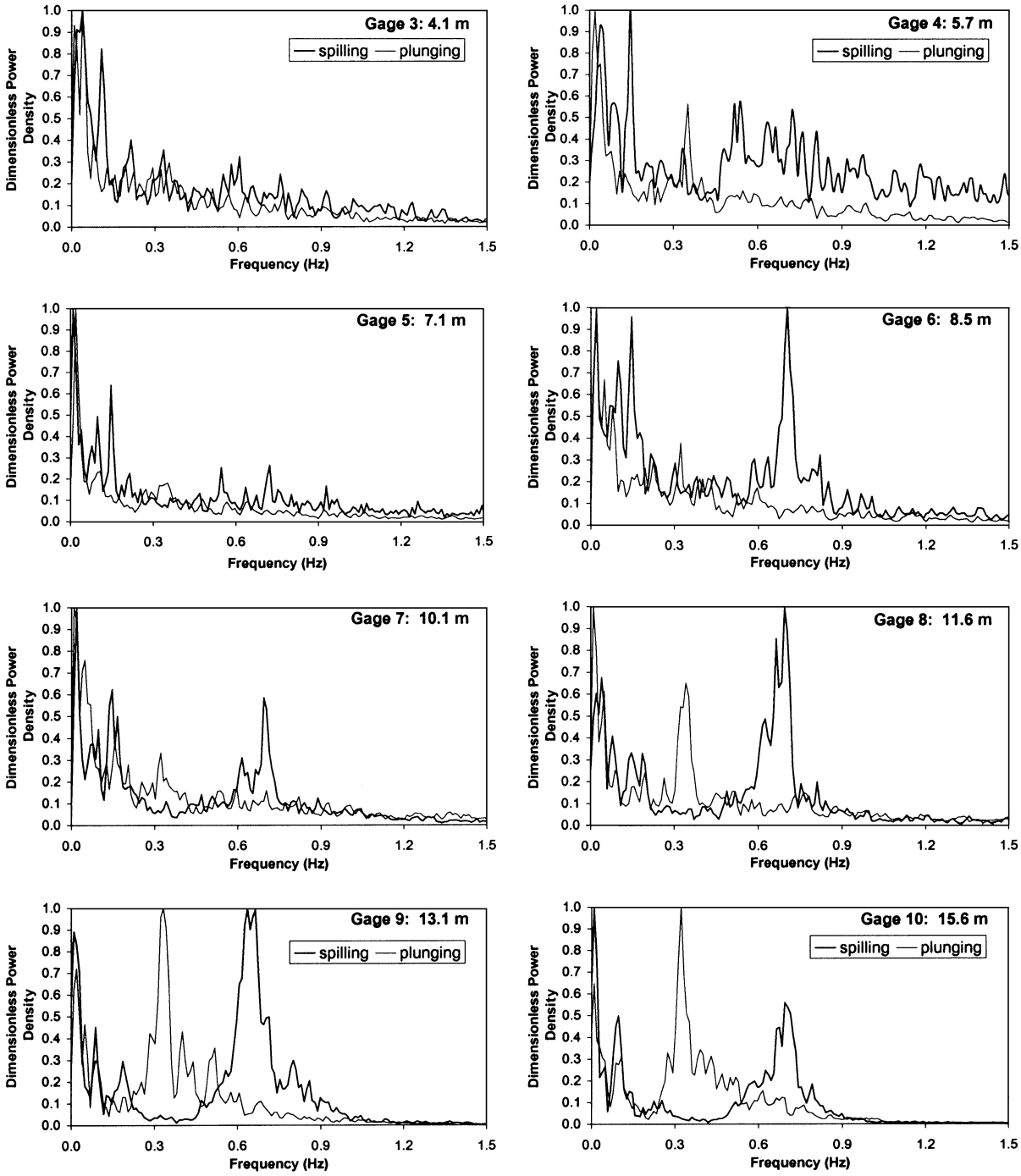

Fig. 8. Spectra of the temporal variations of longshore current.

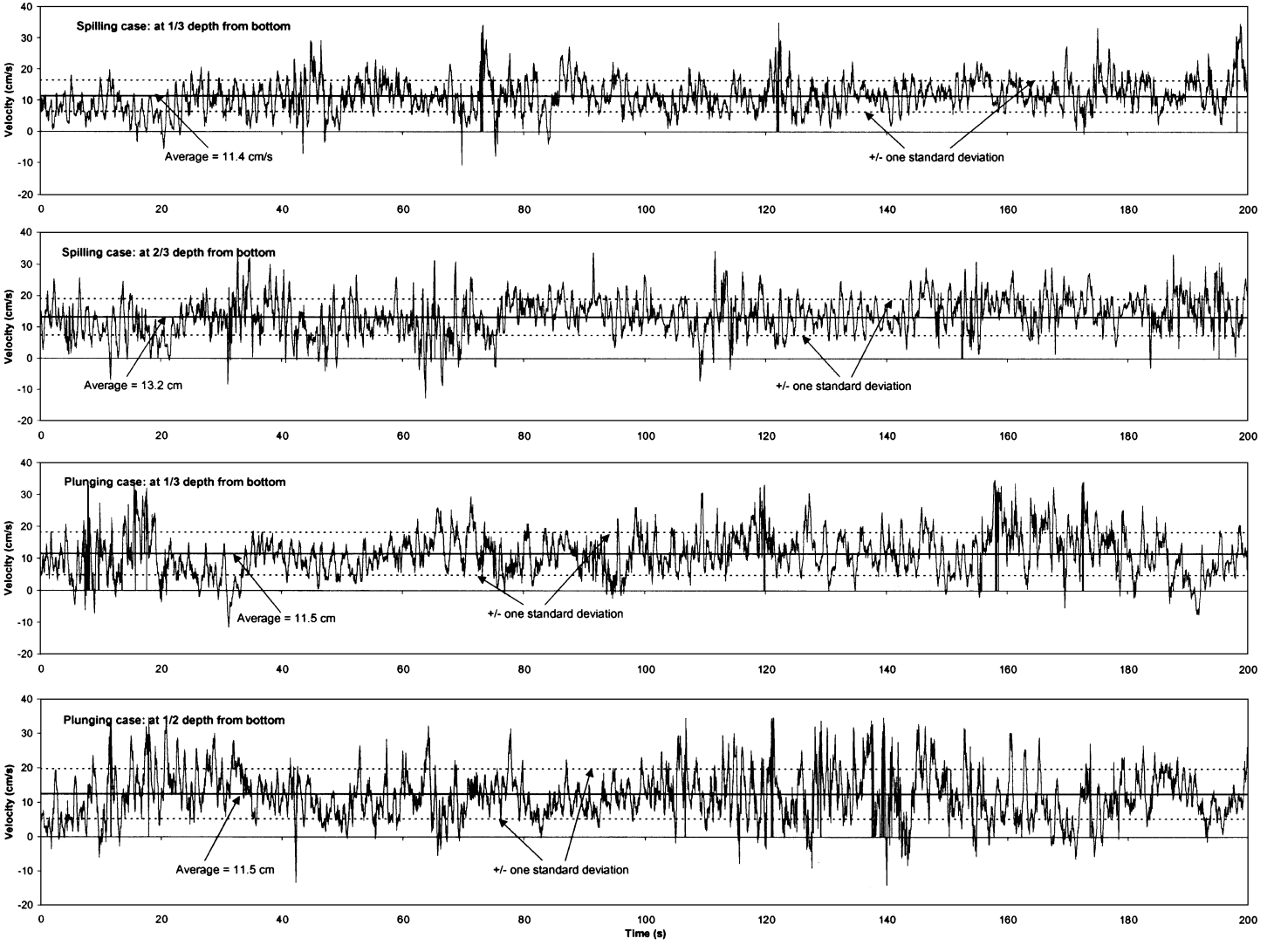

Fig. 9. Time-series longshore current sampled at 20 Hz immediately landward of the main breaker line (at ADV6).

The magnitude of the temporal variations did not vary significantly with sensor elevation throughout the measured water column. The standard deviations at other cross-shore locations in the surf zone were of similar magnitudes (Table 3). The two landwardmost gages are not included in Table 3 due to the spikes probably caused by exposure of the sensors and intensive air-bubble entrainment (Hamilton et al., 2001). Similar ranges of variation were obtained after removal of the spikes.

For the plunging case examples, one standard deviation was about 58% of the mean, indicating slightly more relative variation than the spilling case (Fig. 9, bottom two panels). Similar to the spilling case, the magnitude of the variations was not significantly influenced by vertical elevation across the mid-surf zone. Considerably greater variations were measured near the plunging breaker line (Table 3). This could be influenced by the intense turbulence and also reduced sensor performance due to the substantial air entrainment at the plunging breaker line. Reversal of longshore-current direction occurred only occasionally (Fig. 9).

4.2. Temporal variations and periodicities of sediment concentration

Great temporal variations of suspended sediment concentration, ranging over several orders of magnitude, were measured. Similarly large variations were also reported from field studies (e.g., Beach and Sternberg, 1992; Miller, 1998, 1999; Puelo et al., 2000). Two examples, one each from the spilling (upper panel) and plunging (lower panel) breaker zones at 10.1 m from shoreline, are illustrated in Fig. 10. Sixty-second sections of the 10-min record are shown. Sediment suspension under breaking waves was largely episodic (Fig. 10). Intermittent events of sediment suspension dominated the temporal variation patterns. Sediment concentration varied over a greater range under the plunging breakers than under the spilling breakers with greater sediment concentration measured high in the water column due to the much more active sediment suspension caused by the plunging breakers. Temporal variations of suspended sediment concentration in the mid-surf zone for both cases showed similar patterns as observed at the spilling breaker line.

Close examination of the time series of sediment concentration at the different elevations indicates that the variations were not exactly in phase although qualitatively correlated suspension events at different levels were evident at times. However, large concentration measured at one level sometimes did not have directly corresponding high values at other levels. An example is shown in Fig. 10 (upper panel). The large concentration at 3 cm above bed measured between 208 and 214 s did not have corresponding concentration jumps at other elevations. At the plunging breaker line, greater or similar sediment concentration was occasionally measured at a higher elevation when compared to data from a lower elevation. An example can be found in the lower panel of Fig. 10 between 292 and 295 s, when concentration measured at 21 cm above bed was similar or greater than that measured at 7 cm. A constant phase shift among concentrations at different elevations could not be identified from visual inspection.

Visual observations during the experiments indicated that sediment suspension events were closely related to the detailed spatial patterns of wave breaking. This was particularly apparent for plunging breakers. A cloud of sediment was suspended into the water column at the plunge point and then dispersed across shore. Horizontal advection seemed to play a significant role in dispersing the sediment suspended at the plunging point. The locations of the breaking point for irregular waves were influenced by

Table 3
Temporal variation, as indicated by one standard deviation, of longshore current for the spilling and plunging cases

	Spilling breaker case	Plunging breaker case
	Percentage of the mean value	
ADV3 (4.1 m from shoreline)	49.4 ± 3.9[a]	51.8 ± 6.9[b]
ADV4 (5.7 m from shoreline)	54.3 ± 6.4	61.0 ± 5.4
ADV5 (7.1 m from shoreline)	44.2 ± 2.8	59.5 ± 7.7
ADV6 (8.5 m from shoreline)	42.4 ± 3.2	61.3 ± 8.1
ADV7 (10.1 m from shoreline)	48.6 ± 3.7	92.8 ± 17.3
ADV8 (11.6 m from shoreline)	54.1 ± 11.7	95.9 ± 14.7

Measurements were conducted at 1/3 still-water depth from the bottom.

[a] Values represent the average of nine measurements at different longshore locations, and the alongshore variation.

[b] Values represent the average of four measurements at different longshore locations, and the alongshore variation.

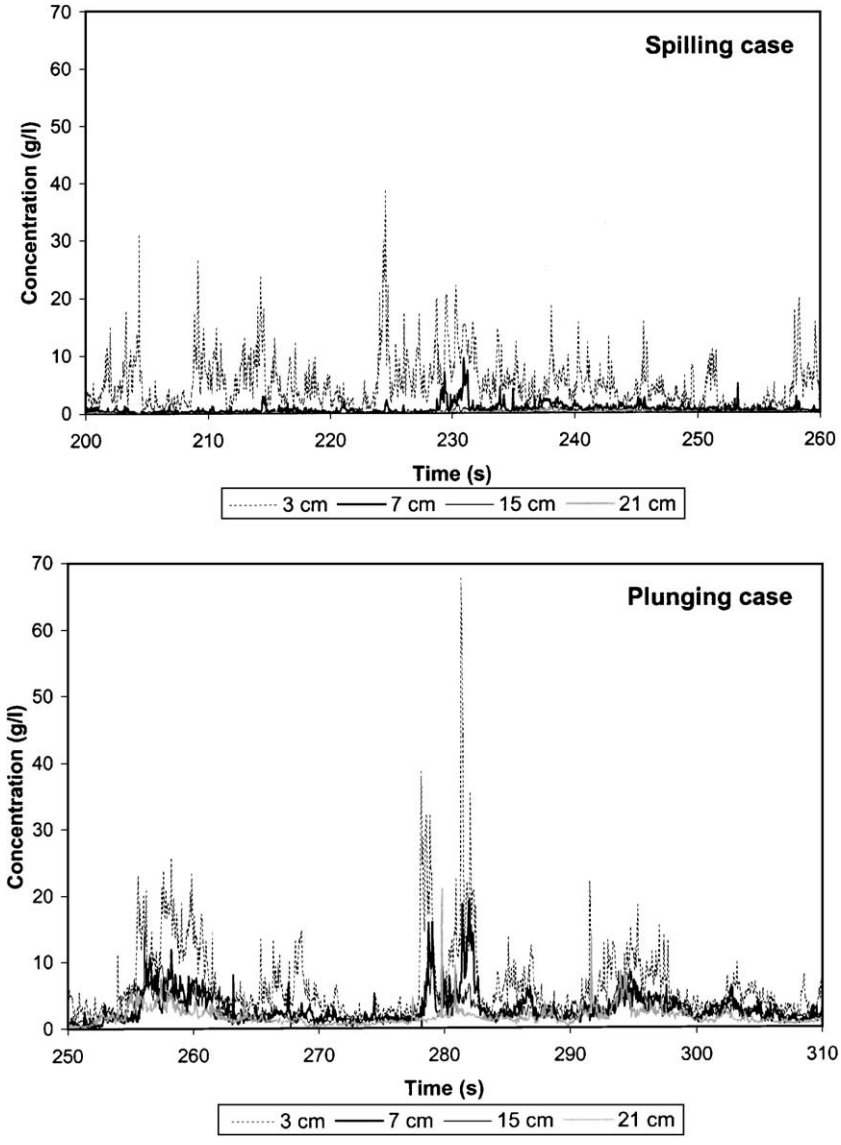

Fig. 10. Time-series sediment concentration at four levels from the bed sampled at 16 Hz for spilling case (upper panel) and plunging case (lower panel). Numbers of centimeters referred to the sensor elevations above bed.

various factors including individual wave height and length, characteristics of wave groupiness, and water depth. Sediment suspension events at a particular location did not necessarily correspond to groups of high waves unless the high waves resulted in wave breaking at that particular location.

Despite the intermittent suspension events in the sediment-concentration record, the same procedures used in the spectral analysis of wave and current data were applied. The purpose was to examine the frequency characteristics of the sediment suspension in comparison with the wave and current patterns. Fig. 11 shows examples of the dimensionless power density of sediment-concentration variations at the spilling (upper panel) and plunging (lower panel) breaker lines (data from same record shown in Fig. 10).

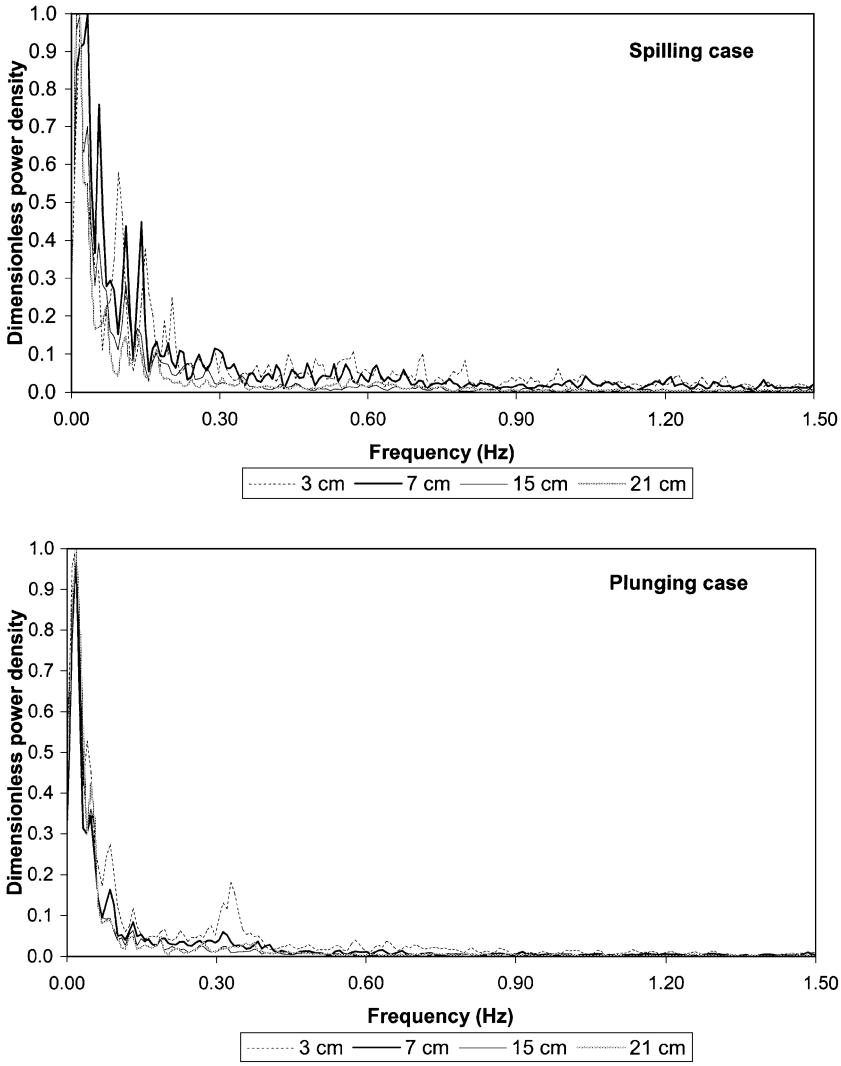

Fig. 11. Spectra of the temporal variations of suspended sediment concentration at the breaker line for spilling (upper panel) and plunging (lower panel) cases.

Overall, the shapes of the power spectral density of sediment-concentration variations are significantly different from those of water-level fluctuation and cross-shore current. Generally, the spectral density did not exhibit a strong peak at the principal incident-wave frequency, i.e., 1.5 s (0.67 Hz) for the spilling case and 3.0 s (0.33 Hz) for the plunging case. The spectra revealed slight peaks for the concentration measured 3 and 7 cm above the bed at the plunging breaker line. At the spilling breaker line, a noticeable wave-frequency peak was only observed at 1 cm above bed (not shown in Fig. 10) and not above this level. Across the mid-surf zone for both spilling and plunging cases, temporal variation of sediment concentration at the incident-wave frequencies can only be identified at 1 cm from bed. These indicate that signatures at the incident-wave frequencies are only evident in the region near the bed. The low-frequency peaks at 50 s (0.02 Hz) to 100 s (0.01 Hz) in the concentration spectra are also artifacts of the present spectral analysis method, similar to those in longshore-current spectra (Fig. 8).

4.3. Spatial variations of surf-zone current

Along the middle 16 m of the test beach, the longshore current, cross-shore current, and sediment concentration showed little variation in the alongshore direction. The following discussion focuses on spatial variations of the time-averaged current in the vertical and cross-shore directions. Typically, 10-min averages corresponding to the duration of the wave-generation drive signal were computed.

4.3.1. Vertical and cross-shore variations of the time-averaged longshore current

Vertical profiles of time-averaged longshore current were obtained at the 10 cross-shore locations (Table 1). A trend of upward increasing current was measured throughout the water column at most locations across the surf zone for both the spilling (Fig. 12) and the plunging (Fig. 13) cases. Current measurements obtained high in the water column at the landwardmost ADV1, and at some of the other locations, could be influenced by the proximity to the surface and intermittent exposure of the sensor. In the upper portion of the water column, nearly 50% of the data points from ADV1 were removed due to unrealistic spikes.

Except at the shallow ADV1 located at 1.1 m from shoreline, the logarithmic curves fit the time-averaged longshore current profiles well. The average correlation coefficient of the least-square curve fitting, R^2, is 0.96 for the spilling case, with a standard deviation of 0.025, or 2.6% of the mean (Fig. 12). Slightly greater scatter was evident for the plunging case, with an average R^2 value of 0.89 and a standard deviation of 0.066, or 7.4% of the mean (Fig. 13). The longshore current is driven by the radiation stress from the obliquely incident waves; the variation over depth is attributable to the effects of bottom stress and the depth-dependent forcing and mixing. Examination of the detailed relationship between the wave forcing and boundary effects and the current-profile shape is beyond the scope of this paper.

Logarithmic mean longshore current profiles are in contrast to the fairly uniform profiles measured over a fixed concrete bed under regular and irregular waves in the same facility (Hamilton and Ebersole, 2001). Relatively uniform longshore current profiles were also measured in the fixed-bed laboratory study of Visser (1991). Longshore current profiles that were nearly uniform with depth outside of a boundary layer were derived in a mathematical analysis of Svendsen and Lorenz (1989) using regular waves. The friction associated with the movable bed and its rippled bedforms appears to have significant influences on the shape of time-averaged longshore current profiles.

Because the current measurements could not be made reliably above the wave-trough level near the water surface, the profiles shown in Figs. 12 and 13 span approximately 65% to 80% of the still-water depth. The depth-averaged longshore current, $V_{\text{d-average}}$, was calculated as

$$V_{\text{d-average}} = \frac{\sum_{i=1}^{N-1} \frac{(V_{i+1} + V_i) \times (h_{i+1} - h_i)}{2}}{(h_{\text{highest}} - h_{\text{lowest}})} \tag{8}$$

where V_i is the current speed measured at the i level; h_i is water depth at the i level; h_{highest} and h_{lowest} are water depths at the highest and lowest measurement levels, respectively; and N is the number of elevations where current measurements were made. Because little is known about longshore current near and above wave trough, no extrapolation was conducted to incorporate the upper 20% to 35% of the water column into the averaging process; therefore, the depth-averaged current calculated from Eq. (8) does not reflect this portion of the water column. Also, the bottom 1 cm was not included in the averaging. If the near-surface longshore current follows the same logarithmic trend, the present calculation (Eq. (8)) would result in an underestimate of the depth-averaged current speed.

The depth-averaged longshore current agreed well with the current speed measured at an elevation of 1/3 still-water depth from the bed, with the differences being within 15% at all cross-shore locations for both spilling and plunging cases (Fig. 14). It is thus concluded that current measurements made at 1/3 depth from bed provide reliable representations of depth-averaged values, excluding the top portion of the water column.

Cross-shore distribution patterns of mean longshore current were remarkably similar for both the spilling- and the plunging-breaker cases. In the cross-

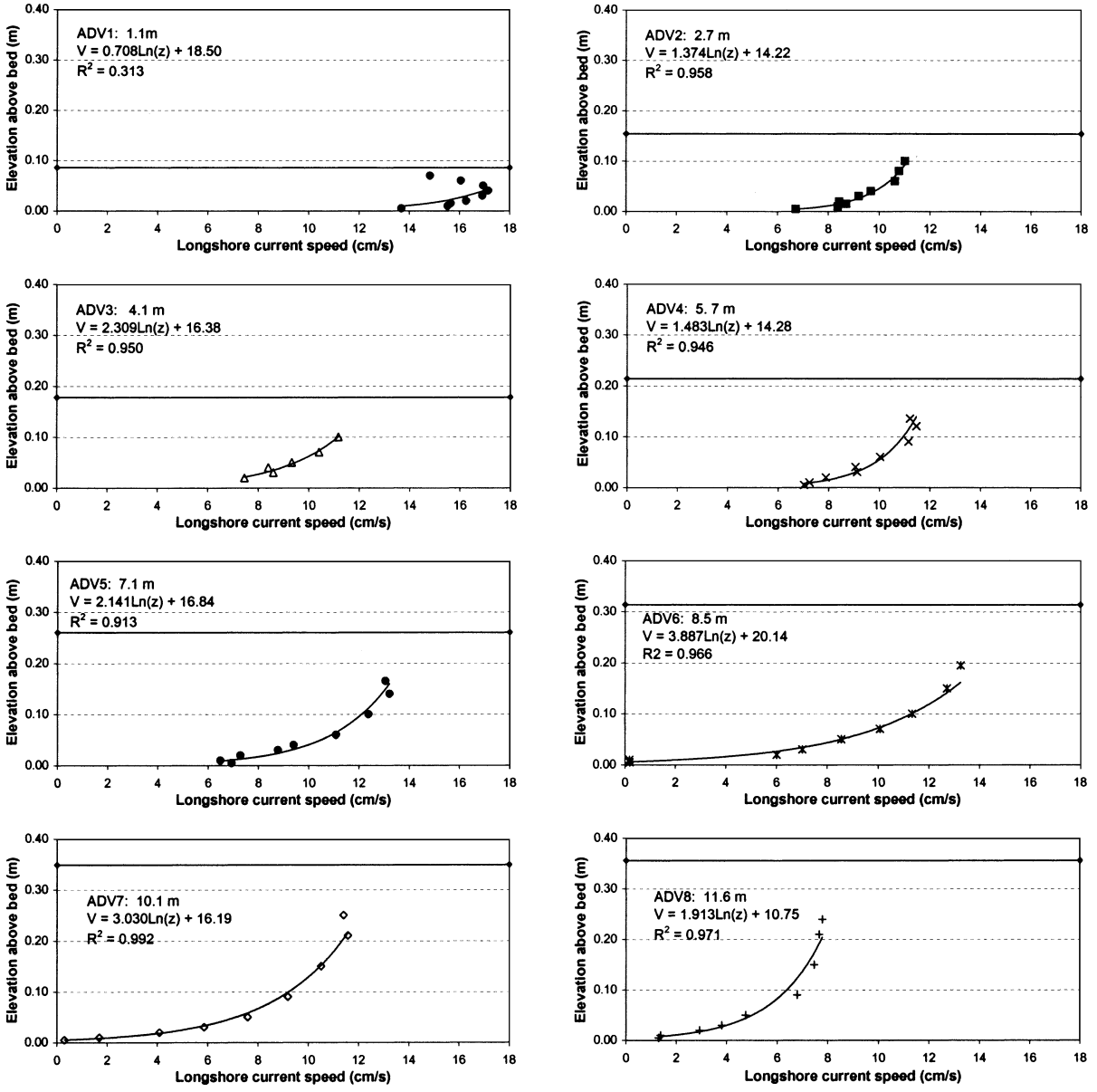

Fig. 12. Profiles of time-averaged longshore current at various locations across the surf zone, spilling case. Solid horizontal line indicates still-water level.

shore direction, the depth-averaged longshore current was nearly constant from 4 to 11 m from the shoreline (Fig. 14). The greatest longshore current speeds were measured at the landwardmost ADV1 at 1.1 m and, in both cases, the current speeds decreased in the seaward direction through the incipient breaker zone from approximately 11 to 15 m. A small reversal in the longshore current was measured at the seawardmost ADV, indicating the presence of recirculation. Minimizing recirculation in the LSTF is discussed in detail in Hamilton and Ebersole (2001).

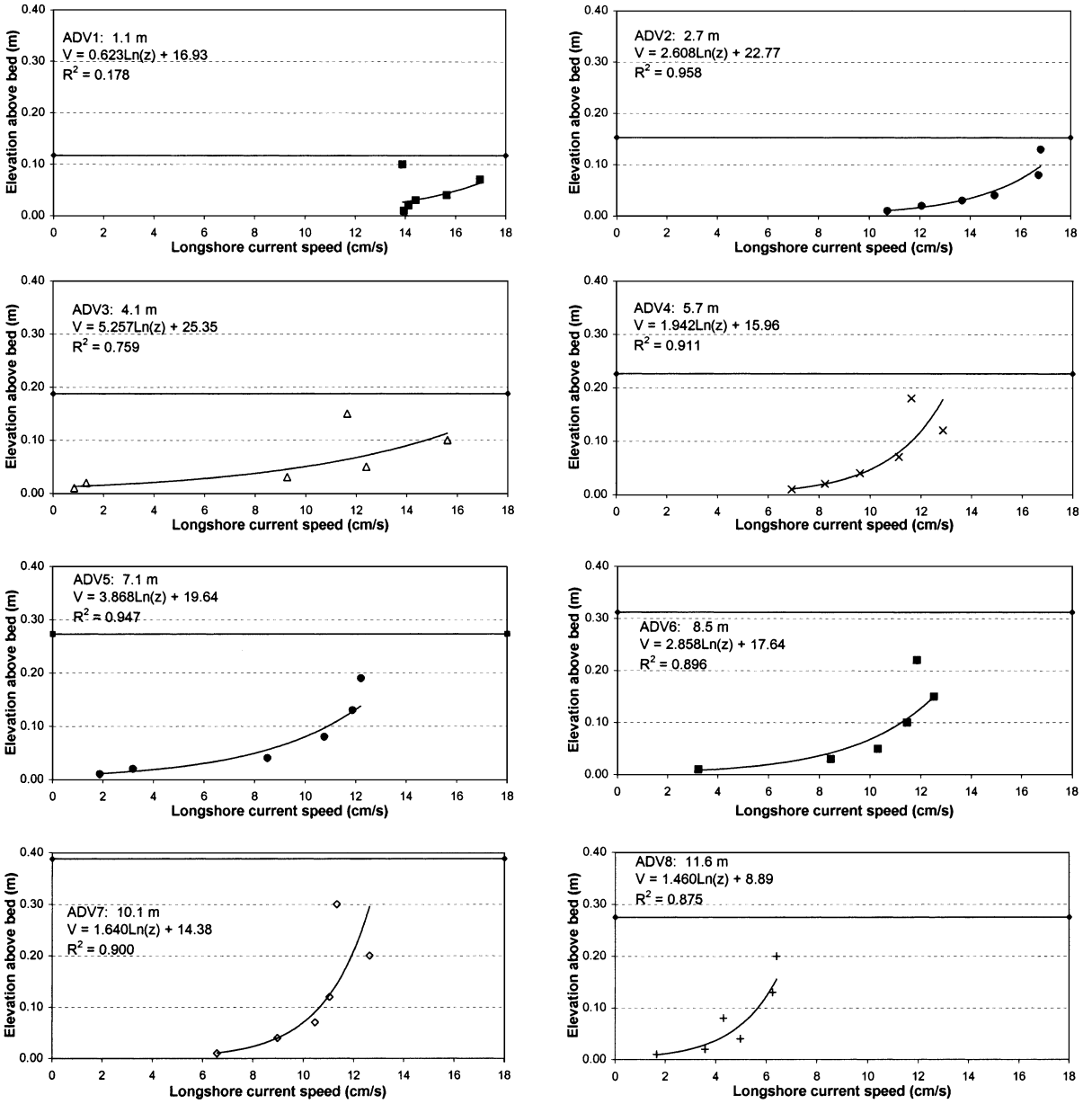

Fig. 13. Profiles of time-averaged longshore current at various locations across the surf zone, plunging case. Solid horizontal line indicates still-water level.

The measured cross-shore distributions of longshore current (Fig. 14) are considerably different from the classic shape, in which the peak current is located a short distance landward of the breaker line, as predicted by the analytical model of Longuet-Higgins (1970) for regular waves and also from measurements made at the LSTF for regular and irregular waves impinging on a planar concrete beach (Hamilton and Ebersole, 2001). Relatively uniform longshore current or patterns with a low, broad peak

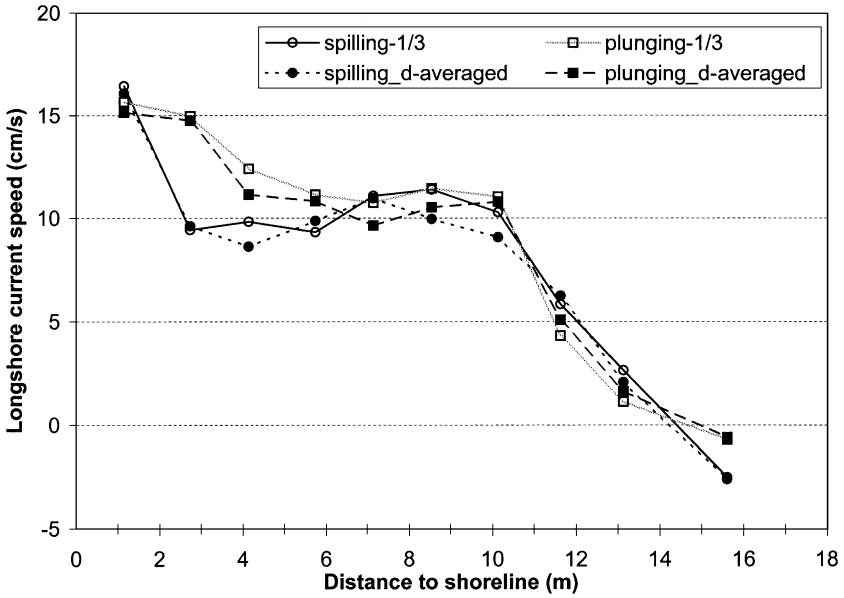

Fig. 14. Cross-shore distribution of longshore current and comparison between depth-averaged velocities and velocities measured at an elevation of 1/3 still-water depth from the bed.

have also been reported from field studies (e.g., Kraus and Sasaki, 1979; Smith et al., 1993). Field data collected by Thornton and Guza (1986) over a dissipative nearly planar beach showed a longshore current peak well within the surf zone.

The similar cross-shore distribution patterns of longshore current measured for these two different wave cases, over considerably different equilibrium beach profiles, indicates that the cross-shore distribution was not significantly influenced by breaker type, even near the breaker line. The vertical current profiles measured across most of the mid-surf zone for both cases were also similar (Figs. 12 and 13).

4.3.2. Vertical and cross-shore variations of time-averaged cross-shore current

The vertical profiles of time-averaged cross-shore current exhibited different shapes when compared to the logarithmic longshore-current profiles. Generally, offshore-directed mean flow was measured in the lower portion of the water column and onshore-directed flow near the water surface. Only a small portion of the onshore-directed flow was measured due to the difficulties associated with collecting data near the free surface. The profiles of time-averaged cross-shore current shown in Figs. 15 and 16 for the spilling and the plunging cases, respectively, emphasize the offshore-directed portion below the wave trough. Provided that the alongshore uniformity assumption is upheld, the unmeasured portion of the water column is assumed to balance the measured undertow in order to satisfy mass conservation.

The peak of the undertow was typically measured between 5 and 10 cm from the bed, or 25% to 45% of the still-water depth from the bottom, at most cross-shore locations. In the plunging breaker zone (ADVs 7 and 8), the peak undertow was approximately 50% greater than that measured in the spilling breaker zone, 7–10 vs. 4–6 cm/s (Figs. 15 and 16). The undertow was also stronger across most of the mid-surf zone for the plunging-wave case.

The shapes of the cross-shore current profiles can be represented reasonably well with parabolic curves (Figs. 15 and 16). A slightly greater deviation from a parabolic shape occurred during the plunging case. The average correlation coefficient of the least-square curve fitting, R^2, for the eight profiles for the spilling case was 0.83, with a standard deviation of 0.13, or 16% of the mean. The average R^2 value

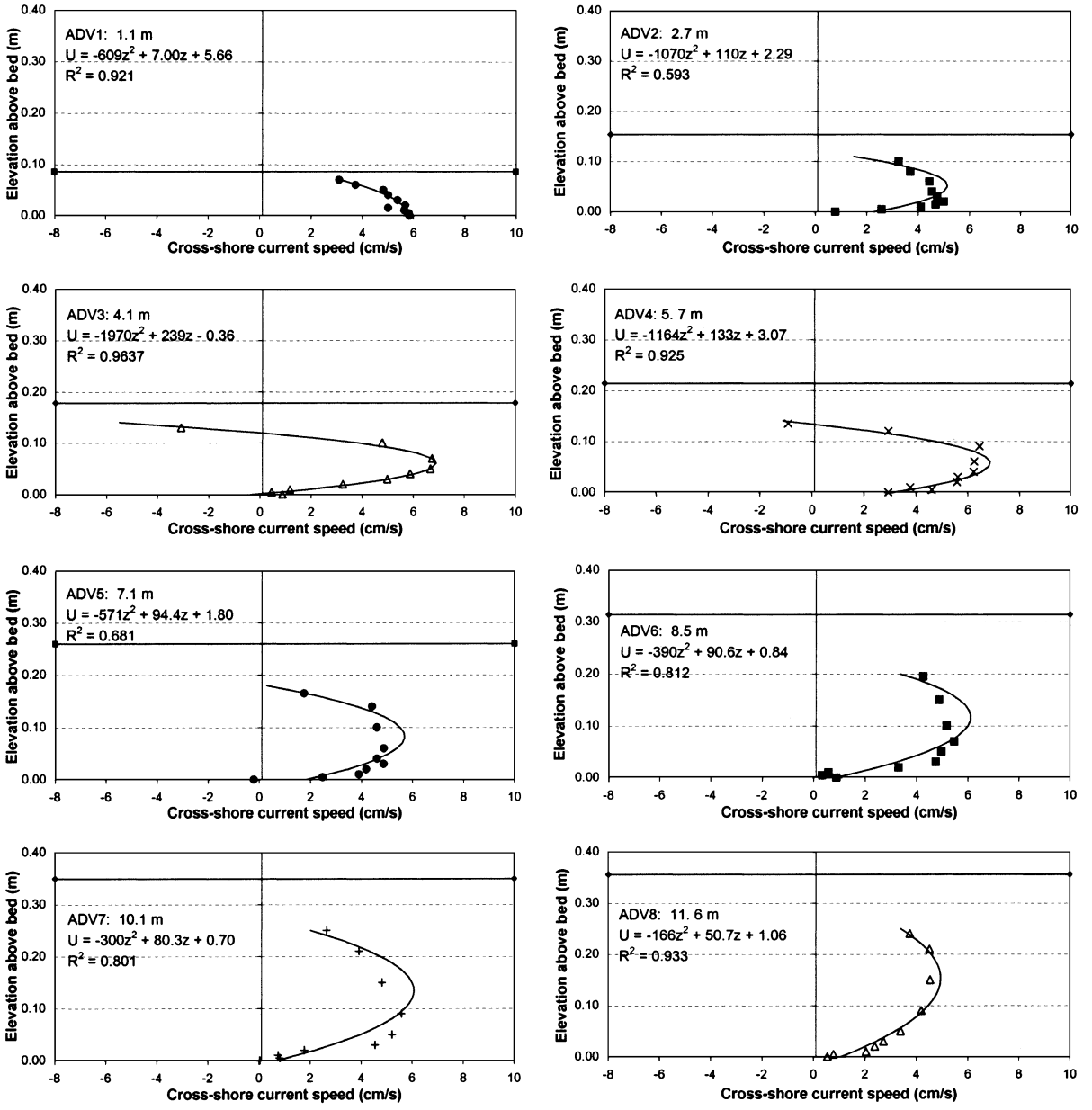

Fig. 15. Profiles of time-averaged cross-shore current at various locations across the surf zone, spilling case. Solid horizontal line indicates still-water level.

for the plunging case was 0.75, with a standard deviation of 0.2, or 27% of the mean. The shape and magnitude of the profiles, as indicated by the best-fit parabola, varied considerably at different cross-shore locations. The undertow is driven by the incident-wave mass flux and the depth-dependent radiation stress; the profile shape is influenced by the bottom stress and vertical mixing. Various models have been developed to predict undertow (e.g., Svendsen and Lorenz, 1989; Garcez Faria et

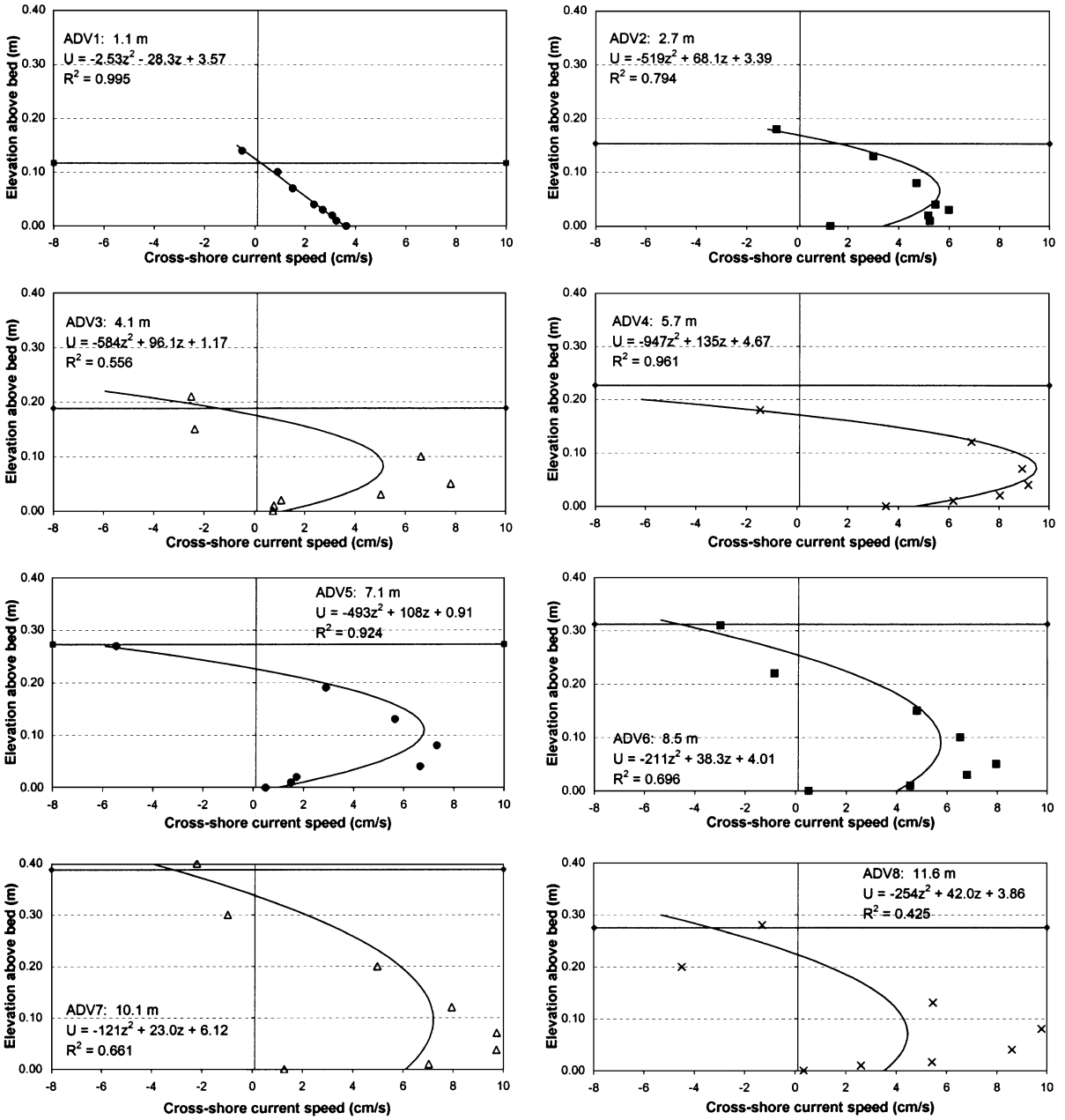

Fig. 16. Profiles of time-averaged cross-shore current at various locations across the surf zone, plunging case. Solid horizontal line indicates still-water level.

al., 2000; Rattanapitikon and Shibayama, 2000), often following the work of Svendsen (1984). Almost all of the models use the wave trough level as the cross-over location between onshore- and offshore-directed water fluxes. The present data agree qualitatively with this location. It is beyond the scope of this paper to examine the details of these undertow models.

4.4. Vertical and cross-shore variations of time-averaged sediment concentration

Time-averaged sediment concentration was greatest near the bottom and decreased rapidly upward through the water column. Fig. 17 shows the time-averaged sediment-concentration profiles across the surf zone for both spilling (upper panel) and plunging (lower panel) cases. Data in Fig. 17 represent average values at various cross-shore locations. Within 3 cm from the bed, the sediment concentration was more than 1 g/l at nearly all cross-shore locations. Above 10 cm from the bed, the suspended sediment concentration was usually less than 0.3 g/l. Above 15 cm from the bottom, the average sediment concentration was generally less than 0.02 g/l. An exception occurred at the plunging breaker line, where suspended sediment concentration above 3 cm from the bed remained

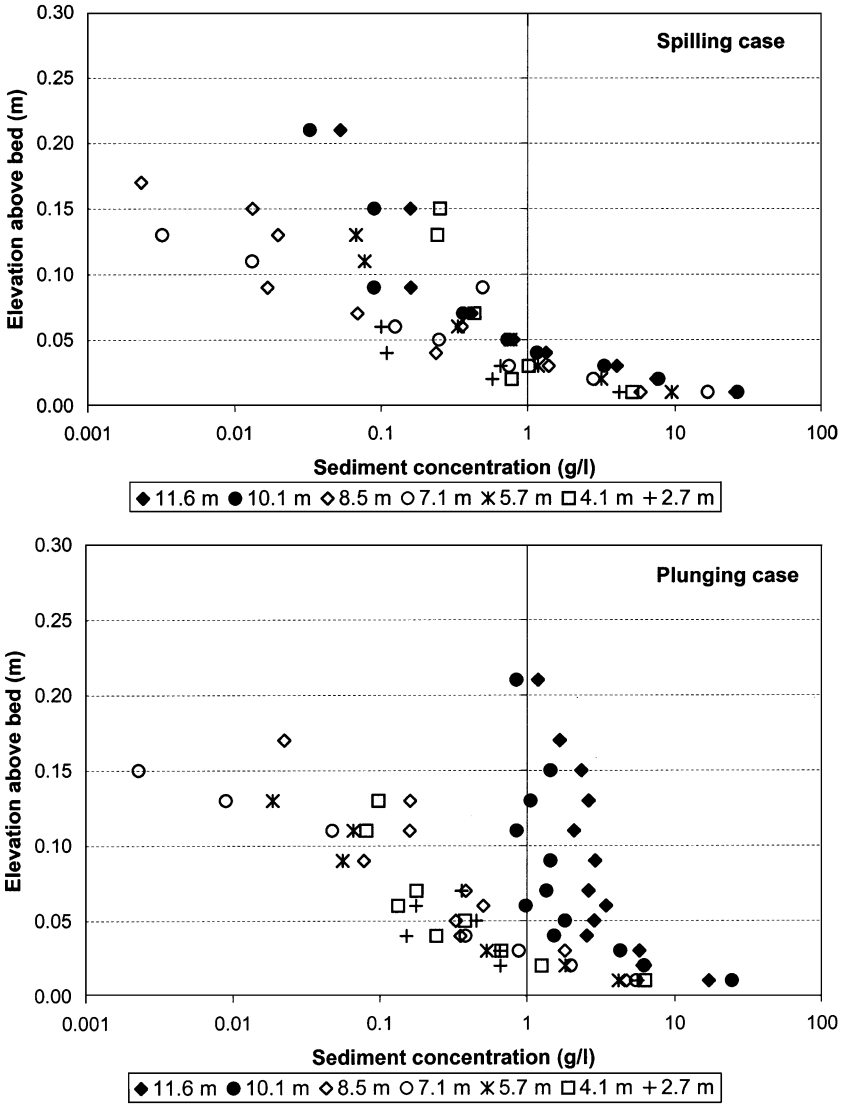

Fig. 17. Profiles of time-averaged suspended-sediment concentration at various locations across the surf zone. Legends indicate distance from shoreline.

nearly constant ranging from 1 to 3 g/l. This nearly uniform sediment concentration at the plunging breaker line is likely related to the intense turbulence and mixing generated by the plunging type of wave breaking and resulting sediment suspension. The slow-settling speed of the fine sand, 1.8 cm/s, also contributes to the nearly homogeneous concentration profile.

A careful examination of the sediment concentration within 5 cm from the bed indicates a general trend of decreasing concentration from the breaker line to the shoreline. In Fig. 18 (also representing average values), sediment concentrations measured at the same vertical elevations but at various cross-shore locations were compared, for both spilling (upper panel) and plunging cases (lower panel). A general decreasing trend from the offshore ADV8 (11.6 m) to the nearshore ADV2 (1.1 m) is apparent. The reasons for this landward decreasing trend are not completely clear, but this is probably related to the reduction in wave energy through the surf zone.

Comparison between the top and bottom panels of Fig. 18 indicates that the near-bottom sediment concentrations were rather similar for the spilling and the

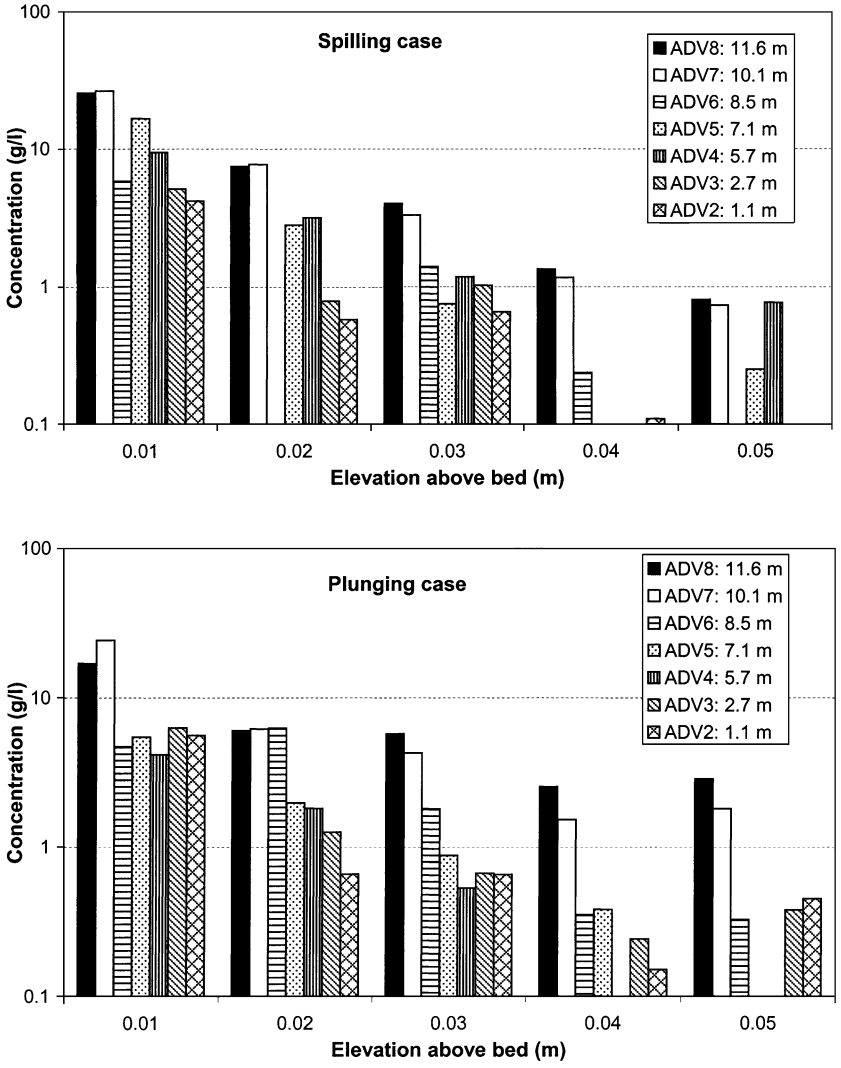

Fig. 18. Comparison of time-averaged suspended sediment concentration within 5 cm from the bed at various locations across the surf zone.

plunging cases. This similarity across the mid-surf zone is reasonable due to similar bed (Fig. 5) and saturated wave conditions (Fig. 2). The mid-surf zone was dominated by surf-bore motions for both cases. Fig. 19 shows root-mean-square cross-shore current ($U_{b\text{-}rms}$) at 3 cm above bed for both cases. Given the small incident-wave angle, $U_{b\text{-}rms}$ should be dominated by the wave-orbital motion. Near-bottom velocity, which determines the bottom shear stress, is one of the dominant factors in sediment suspension (Nielsen, 1992). Despite the differences in wave period, $U_{b\text{-}rms}$ in the mid-surf zone are similar for both cases, apparently regulated by the shallow water depth.

The remarkable similarity in the time-averaged sediment concentration at the spilling and the plunging breaker lines (at ADVs 7 and 8), especially within 3 cm from the bed, is intriguing. To emphasize this similarity, the data in Fig. 18 were rearranged in Fig. 20. Similar sediment concentrations were measured at elevations of 1, 2, and 3 cm from the bed for both spilling (solid bar) and plunging (clear bar) cases; while high in the water column, e.g., at 15 cm from the bed, concentrations measured under plunging breakers were more than one order of magnitude greater than under the spilling breakers (Fig. 20). The water depth and bottom conditions were substantially different at the breaker lines. The still-water depth was nearly 30% shallower at the top of the bar under the plunging breaker compared to the spilling breaker. Under the plunging breakers, the bed elevation changed drastically in the vicinity of the breaker-point bar, from seaward sloping to landward sloping.

Another important factor controlling sediment suspension is the bottom condition, which has strong influence on the bed roughness (e.g., Wikramanayake and Madsen, 1994a,b). Different bed forms were measured under the plunging and spilling breakers especially in the vicinity of the breaker line (Fig. 5). For the plunging-wave case, large, irregular ripples occurred on the seaward slope, and a relatively flat, featureless bed dominated the bar's crest and landward slope. Under the spilling breakers, the bed elevation remained relatively constant and the surface was covered with reasonably regular ripples with heights of 1.0 to 1.2 cm and lengths of 6 to 9 cm.

The hydrodynamic conditions at the plunging and spilling breaker lines were also different with much more turbulence generation during the plunging breaking than during the spilling breaking, with the leading edge of the plunging breaker seemingly impinging directly on the bottom. These substantial differences in bed and turbulence conditions resulted in remarkable differences (over one order of magnitude) in suspended sediment concentration throughout the upper 80% of the water column. Based on present understanding of sediment–fluid interaction, the rel-

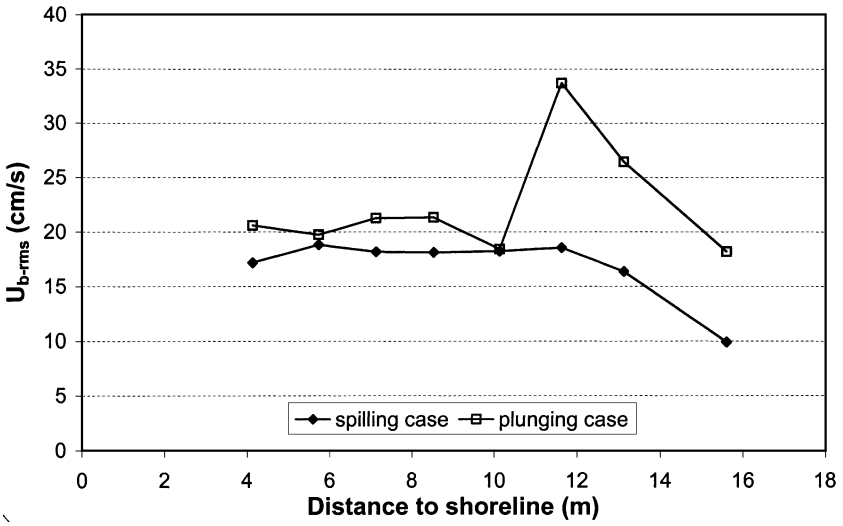

Fig. 19. Root-mean-square of cross-shore current at 3 cm above bed, for the spilling and plunging cases.

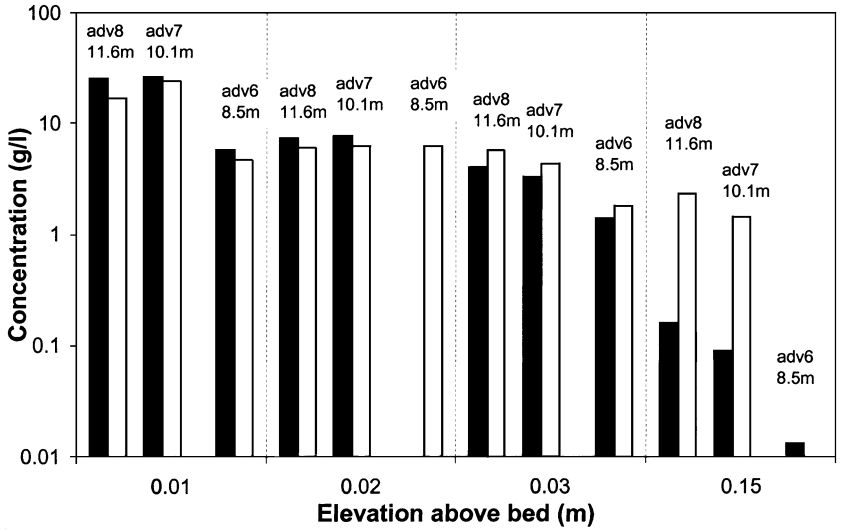

Fig. 20. Comparison of near-bed sediment concentration in the breaker zone between spilling (solid) and plunging case (clear).

atively featureless bed in the vicinity of the plunging breakers indicates a sheet-flow condition and was very different from the rippled bed regime under the spilling breakers. The relatively large near-bed velocity of 34 cm/s also supports the presence of a sheet-flow regime.

The $U_{b\text{-}rms}$ (Fig. 19), measured at ADV 8 (11.6 m) at an elevation of 3 cm from bed, was much greater under the longer-period plunging breakers than under the spilling breakers, 34 vs. 19 cm/s. A sharp drop of $U_{b\text{-}rms}$ was measured in shallower water at ADV7 (10.1 m) for the plunging case, resulting in a similar value with the spilling case. The vertical profile of the root-mean-square (rms) velocity at ADV8, which was located immediately seaward of the bar crest where larger waves broke, was considerably different from the rms-velocity profiles measured at other cross-shore locations (Fig. 21). An upward decreasing trend, instead of an upward increasing trend, was measured. This probably resulted from wave deformation as it propagates over the bar. The rms-velocity profiles measured at ADV7 (10.1 m) and landward were rather similar for both the spilling and the plunging breakers, agreeing with the similar near-bottom velocities (Fig. 19). The seemingly improbable similarity in near-bed sediment concentration and the vast difference throughout most of the water column highlight the lack of understanding between the fluid flow and the sediment concentration under breaking waves.

Nearly identical near-bed, time-averaged sediment concentrations were measured by Nielsen (1979), and summarized in Nielsen (1992, p. 219), for nonbreaking waves and spilling breakers. A conclusion was drawn that except for the extreme case of a plunging jet hitting the bed, the pickup rate at the bed and hence the near-bed sediment concentration was not affected by the spilling breaking. Nielsen (1992, p. 219) further concluded that the main effect of the turbulence from wave breaking is a vertical stretching of the concentration profile, i.e., greater concentration high in the water column. Data from these two LSTF experiments seem to indicate that even when the plunging jet was hitting the bed, the near-bed sediment concentrations, albeit landward and seaward of the predominant plunging point, were still remarkably similar. Nearly identical near-bed, time-averaged concentrations were also measured by Bosman (1982), and summarized in Van Rijn (1993, p. 8.18–8.19), under nonbreaking waves, spilling breakers, and plunging breakers. Bosman (1982) used direct pump-suction samplers instead of optical sensors. No interpretation for the "approximately constant" near-bed concentrations was provided.

Average sediment concentration over the measured part of water column ($C_{a\_water\_column}$) was calculated

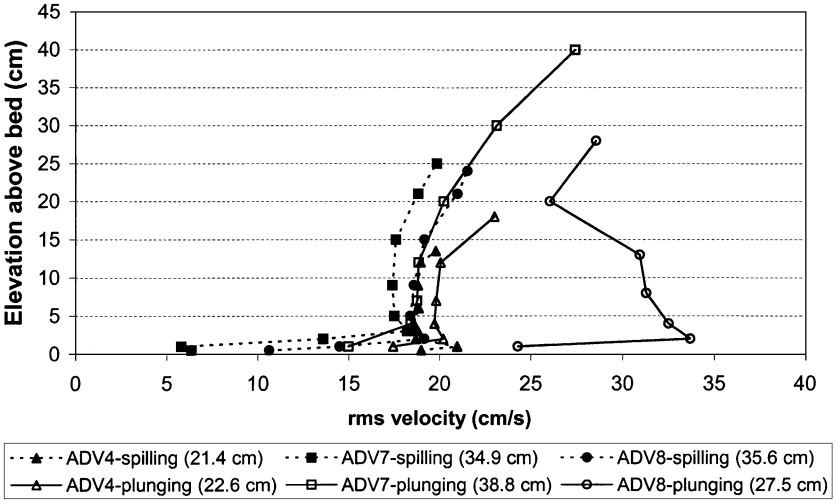

Fig. 21. Vertical profiles of rms velocity at various cross-shore locations for both spilling and plunging cases. Numbers in the parentheses indicate the still-water depth.

using a formulation similar to Eq. (8). It is worth emphasizing that $C_{a\_water\_column}$ provides one estimate over a rapidly upward-decreasing trend that spans up to 4 orders of magnitude. Caution should be exercised when using the depth-averaged sediment concentrations. Nevertheless, averaged values over the measured part of the water column are used in the following to demonstrate a general cross-shore variation of sediment concentration in the surf zone. Although the bottom sensor was deployed directly on the bed, it functioned mainly as an elevation reference for the rest of the sensors, instead of measuring sediment concentration at the bed. The concentration obtained from the bottom sensor was questionable and was not included in the depth averaging. The $C_{a\_water\_column}$ included positions from 1 cm above the bed and spanned over the range of measurements. Near the water surface above the wave trough, the measurements have greater uncertainty due to the varying water depth and frequent exposure of the sensors. No extrapolation toward the water surface was conducted. The $C_{a\_water\_column}$ discussed in the following did not include the top 20% to 35% of the water depth. Given the rapidly upward-decreasing sediment concentration, the exclusion of the upper 20% to 35% water column could result in considerable overestimation of average values. On the other hand, the exclusion of the bottom 1 cm of water column, where the sediment concentration is the greatest, could cause an underestimation of average values.

Although the suspended sediment concentrations at the plunging breaker line above 3 cm from the bed were more than one order of magnitude greater than that in other parts of the surf zone (Fig. 17), the $C_{a\_water\_column}$ was only three to five times greater due to the similar near-bed concentrations. The $C_{a\_water\_column}$ across most of the surf zone remained relatively uniform, ranging from 0.5 to 1.2 g/l for both spilling and plunging cases (Fig. 22). A similar general magnitude of surf-zone suspended sediment concentration, 0.5 to 1.0 g/l, was obtained by Kana (1979) and Zampol and Inman (1989) in the field using instantaneous bottle samplers. The $C_{a\_water\_column}$ at the spilling breaker line were approximately 1.5 g/l; at the plunging breaker line, the $C_{a\_water\_column}$ were approximately 2.5 g/l (Fig. 22). Across most of the mid-surf zone, the $C_{a\_water\_column}$ was slightly greater under spilling breakers than under the plunging breakers. The reason for this is not clear. Sediment concentrations measured at an elevation approximately equal to 20% of the water depth from the bed matched the $C_{a\_water\_column}$ values (excluding the bottom 1 cm and the top 20% to 35% water depth) reasonably well (Fig. 22). The sediment concentration at 1/3 of the still-water depth, where representative current meas-

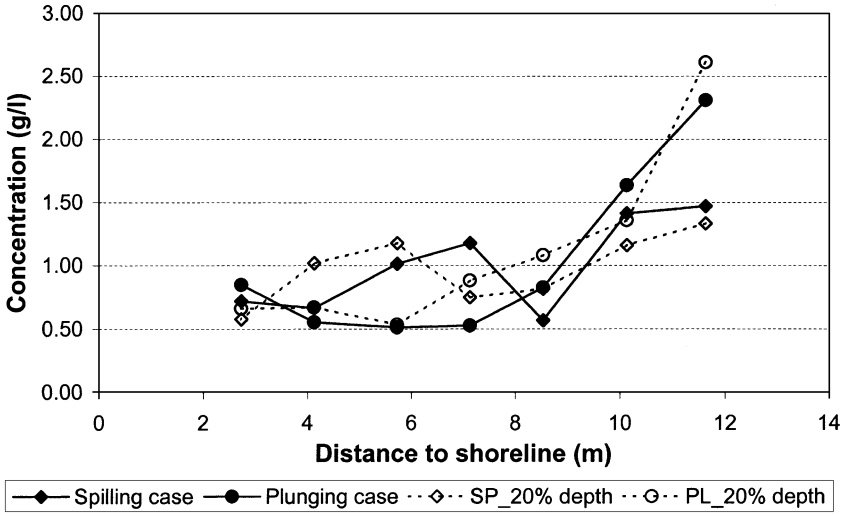

Fig. 22. Time- and depth-averaged sediment concentration, compared with measurements at an elevation of 20% water depth from bed.

urements were taken, was significantly lower than the depth-averaged concentration.

4.5. Calculating sediment flux from current velocities and sediment concentrations

Eq. (1) yields a point value of sediment flux in space and time. It is necessary to integrate the point values over space and time to obtain a sediment transport rate for practical use in coastal engineering and science. Knowledge of temporal and spatial distribution patterns is critical in performing the integration and selecting proper temporal and spatial scales. As discussed in the previous sections, longshore and cross-shore currents and sediment concentrations vary rapidly and differently in time and space. This makes the integration, potentially, very complicated over a realistic domain.

Sediment flux is typically calculated via Eq. (1) using velocity and concentration data obtained from flow and turbidity sensors, respectively. Due to the high costs of sensors and field operations, temporal and spatial coverage is often limited. Miller (1998, 1999) obtained a unique set of storm data in the surf zone with simultaneous measurements of velocities and sediment concentrations at Duck, NC. The 500-m-long concrete pier and a 70-ton crane, allowed measurement to be made under breaking waves of nearly 4 m high.

Limited by the paucity of field and laboratory data and the incomplete understanding of surf-zone processes, present models are not yet capable of precisely predicting instantaneous surf zone velocities and sediment concentrations. Temporally and spatially averaged values are used in most modeling efforts. As discussed earlier, by partitioning the surf-zone current and sediment concentration into mean, high-frequency and low-frequency components (Eqs. (3) and (4)), calculation of time-averaged sediment transport (still in a single point) can be obtained from Eq. (5). Application of Eq. (5) in sediment transport modeling is difficult due to our limited abilities in predicting current and sediment concentration at a temporal scale comparable to the frequencies of gravity and infragravity waves. In the following, possibilities and uncertainties of further simplification of Eq. (5) are examined by considering only the time-invariant terms.

Neglecting the time-varying contributions, i.e., the last two terms on the right-hand side of Eq. (5), can be justified under two conditions. Condition one is satisfied when either the temporal variation of one or both of the two parameters, i.e., the $u_{\_high}$ and $u_{\_low}$ or $c_{\_high}$ and $c_{\_low}$, over the averaging period are sufficiently small compared to the average values. Condition two is satisfied when u and c are independent random variables with a zero mean and the time averages of $u_{\_high} \times c_{\_high}$ and $u_{\_low} \times c_{\_low}$, are negligible.

4.5.1. Longshore sediment flux

Due to limitations of the data acquisition systems, synchronized simultaneous measurements of instantaneous sediment concentration and velocity throughout the water column and at different cross-shore locations could not be achieved. Therefore, true values of instantaneous longshore sediment flux could not be computed directly from the product of velocity and concentration (Eq. (1)). In addition, longshore currents were sampled at 20 Hz, while concentrations were sampled at 16 Hz. In order to adopt Eq. (1) to estimate instantaneous sediment flux, the velocity and concentration data were resampled at 4 Hz, which was chosen to avoid data interpolation. Different artificial instantaneous sediment flux time series were computed in which the first point of the longshore current record was first matched with the second point of the concentration record, then matched with the third and fourth point of the concentration record, etc. In this way, the concentration time series were shifted relative to the velocity record by a constant time of 0.25 s at each step. A set of 48 artificial instantaneous longshore sediment flux calculations spanning a total time shift of 12 s was obtained. Because the velocity measurement was started within 3 ± 2 s after the concentration sampling, one of the shifted flux values should closely represent the product of the simultaneous u and c. Each of the 48 instantaneous flux time series was averaged over the 10-min sampling interval and then compared with the flux obtained from the product of time-averaged velocity and time-averaged concentration. If the averages of all 48 artificial instantaneous fluxes (with one representing the true value) are reasonably constant and compare well with the flux obtained from time-averaged longshore current and time-averaged concentration, it is then reasonable to believe that the first term in Eq. (5) provides an acceptable estimate of longshore sediment flux at a specific elevation in the water column. Partitioning the current and concentration (Eqs. (3) and (4)) into high- and low-frequency components is a fairly complicated procedure and is being examined in a separate study.

Fig. 23 plots the 48 flux estimates in terms of the percentage difference from the flux obtained from the product of time-averaged longshore current and time-averaged concentration. The upper panel shows results from the spilling case, and the lower panel shows results from the plunging case. Several representative locations, horizontally and vertically in the water column, are shown in each panel. Results at other horizontal and vertical locations are comparable. Overall, the differences were small, mostly within $\pm 8\%$ for the spilling case. For the plunging case, the differences were slightly greater although still mostly within $\pm 12\%$, with a few points exceeded 15%. These results suggest that longshore sediment flux obtained from the product of time-averaged longshore current and time-averaged sediment concentration provides a good estimate of the temporal average of instantaneous longshore sediment flux. The maximum uncertainty caused by neglecting the time-variant contributions should generally be within $\pm 12\%$ for both cases. The relatively small contribution from the time-variant portions to the averaging is probably because temporal variations of longshore current are fairly small relative to the average values (Fig. 9) and also because the time variations of longshore current and sediment concentration were largely independent, which should result in a near-zero average product. It is worth noting that the above conclusion was reached in light of the fact that longshore current was not significantly influenced by individual wave motions. Under larger breaker angles, this may not be the case.

The product of time-averaged profiles of longshore current and sediment concentration yields an estimate of the suspended sediment-flux profile through the water column. Within 3 cm from bed, measurements of sediment concentration and longshore current were conducted at the same elevation, at 1-cm intervals. Minor differences (less than 3 cm) in measurement elevations existed in the upper portion of the water column. Because the vertical gradient of sediment concentration was much greater than that of longshore current, the longshore currents were linearly interpolated to match the levels of the sediment concentration measurements where necessary.

The resultant sediment-flux profiles exhibit a rapidly upward-decreasing trend, except at the plunging breaker line, where a relatively uniform flux was obtained throughout the water column above 4 cm from bed. In the breaker zone, both the shapes and the magnitudes of the sediment-flux profile were significantly different for plunging and spilling cases

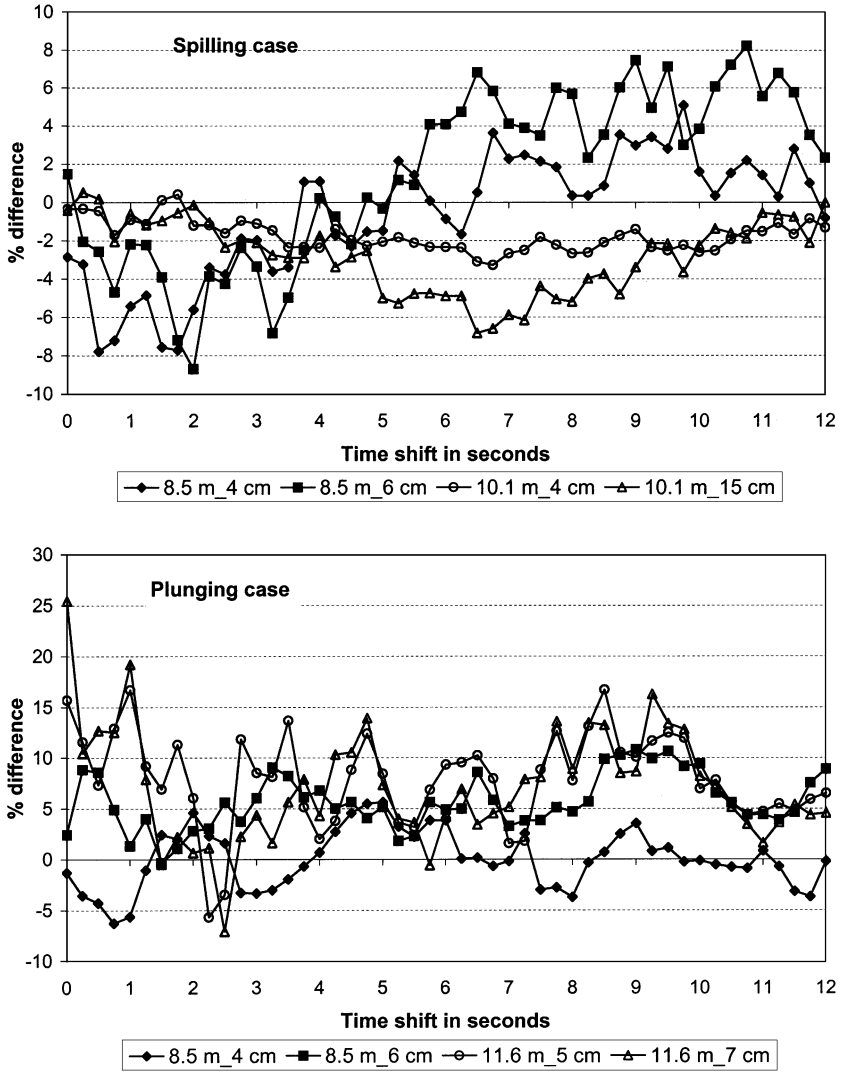

Fig. 23. Time averages of the "shifted" longshore flux in comparison with flux obtained from the product of time-averaged longshore current and time-averaged concentration. Legends refer to distance from the shoreline and sensor elevation.

(Fig. 24, upper panel). While in the mid-surf zone, the sediment-flux profiles were similar (Fig. 24, lower panel). The shapes of sediment-flux profiles resemble those of sediment concentration (Fig. 18), apparently dominated by the much more drastic upward decrease of concentration, which overwhelmed the relatively slow upward increase of longshore current. At most cross-shore locations, over 70% of the total longshore sediment flux occurred within 5 cm from the bed, except at the plunging breaker line where less than 30% of the total longshore flux occurred within this portion of the water column. The shapes of sediment-flux profiles have been studied by Kraus and Dean (1987), Kraus et al. (1988), and Wang (1998). A generalized empirical shape for the surf zone sediment-flux profile was derived based on field data collected using streamer sediment traps (Kraus, 1987; Wang, 1998). The profiles obtained in this

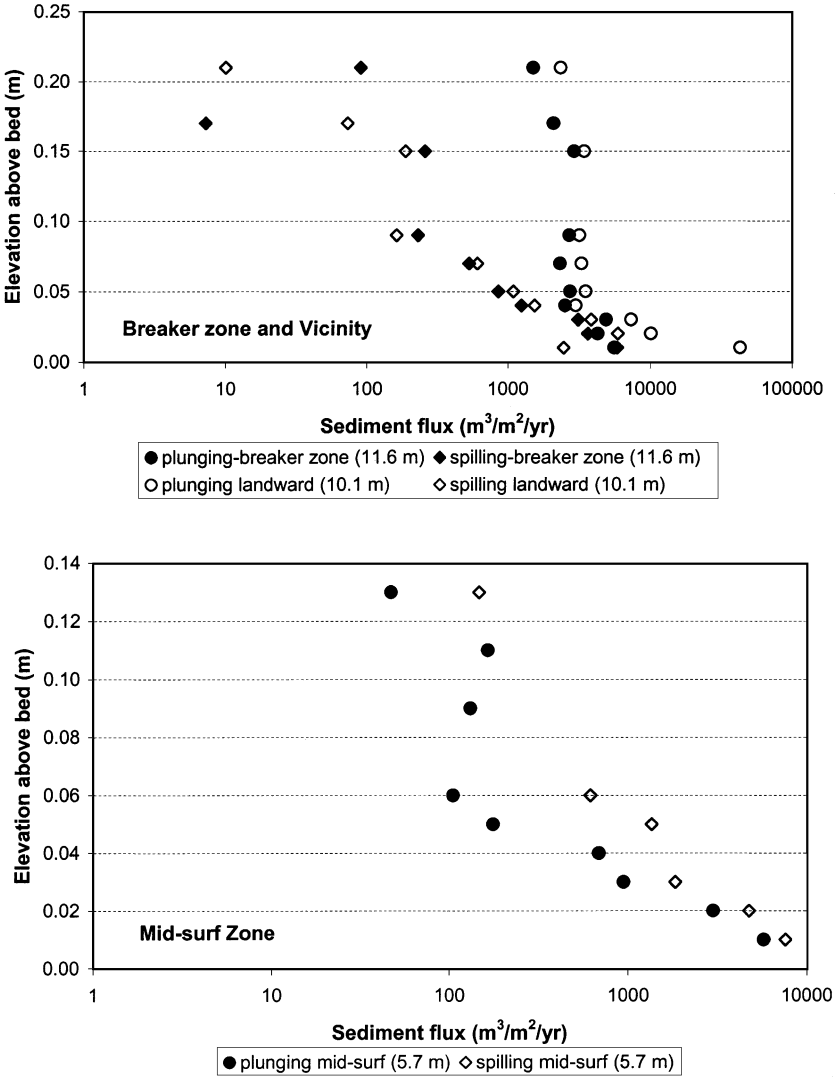

Fig. 24. Sediment-flux profiles obtained from the product of time-averaged profiles of longshore current and sediment concentration.

laboratory study, however, do not compare well with the generalized shape derived from the above field studies. Profiles at the plunging breaker line are steeper as compared to the generalized shape, while profiles at the spilling breaker line and in the mid-surf zone are gentler.

Total sediment flux across a unit width of the surf zone was calculated by integrating the flux profile through the water column. This depth-integrated flux was compared with the sediment flux measured at the downdrift traps. The downdrift traps provide accurate measurement of time- and depth-integrated sediment flux across a 0.75-m section of the cross-shore profile. If the integrated total flux compares well with the measured total flux at the traps, this would provide additional evidence that the product of time-averaged velocity and time-averaged concentration yields reasonable estimates of time-averaged longshore sediment flux. It is worth noting that sediment flux could not be calculated within 1 cm from the bed. Because

little is known within 1 cm of the bed, no estimate of the near-bed sediment flux was made. Also, the sediment flux was not calculated near the water surface. Therefore, the integrated sediment flux did not include the transport that occurred within 1 cm from the bed and the upper 30%, or so, of the water depth.

Overall, the cross-shore distribution of the calculated longshore sediment flux compared reasonably well with the measured flux at the downdrift traps (Fig. 25). These fluxes calculated from the product of time-averaged current and concentration profiles are denoted "profile integration" in the figures. The large longshore flux at the plunging breaker line was reproduced well. Sediment flux across the entire mid-surf zone was significantly underpredicted for the plunging case. The flux at the spilling breaker line was overestimated. Reasons for this overestimation are not clear. For the spilling-breaker case, sediment flux across most of the mid-surf zone was reproduced reasonably well, except close to the shoreline, where an underprediction occurred. Because certain flux contributions near the bed and water

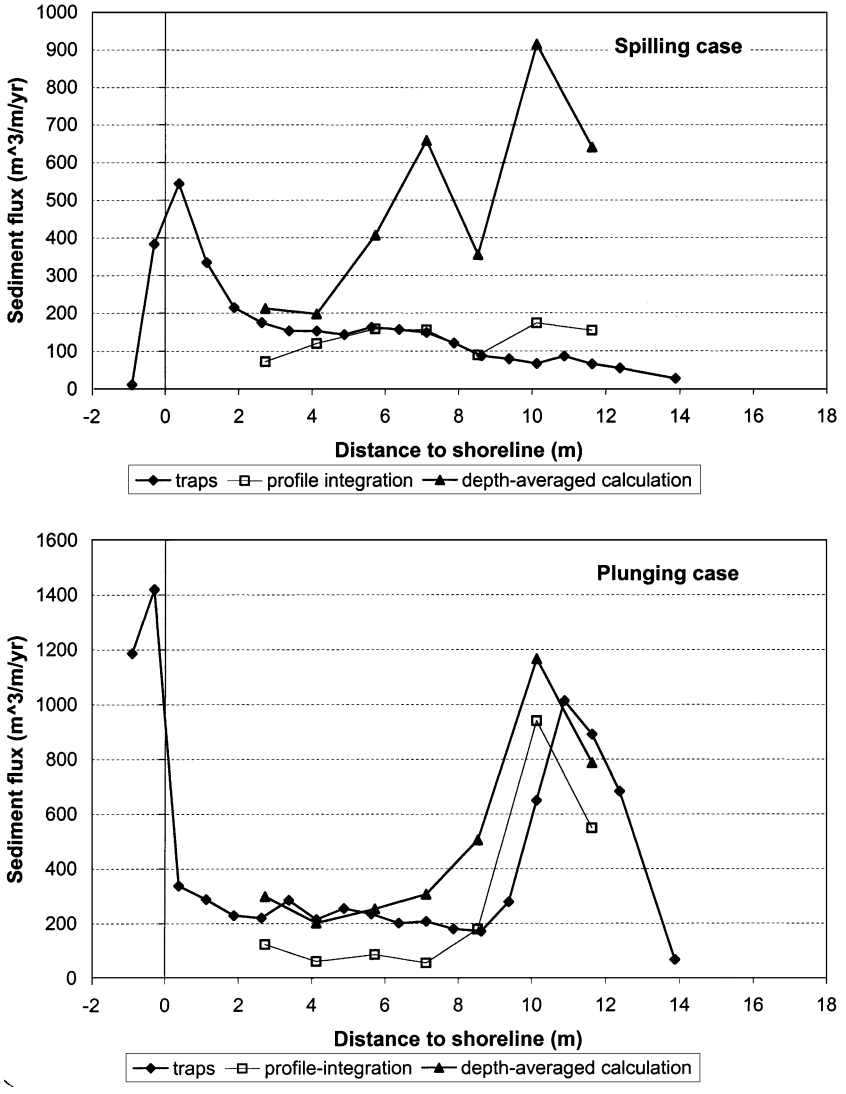

Fig. 25. Comparison of sediment-flux distribution measured at the downdrift traps, integrated over depth, and calculated values.

surface were neglected from the calculation, one would expect the calculated results to be less than the trapped quantities in all cases. For the spilling case, the total sediment flux measured at the bottom traps across the section of beach from 2.7 to 11.6 m (from the shoreline) was 1200 m^3/year, the same as the 1200 m^3/year calculated from the profiles of time-averaged longshore current and sediment concentration. However, for the plunging case, the total sediment flux was 3600 m^3/year for the traps and 2500 m^3/year, or approximately 30% less, for the calculated rate from 2.7 to 11.6 m. The underprediction resulted from the lower calculated values across the mid-surf zone.

Given the uncertainties involved in using the time-averaged longshore current and sediment concentration, and the neglect of transport in the bottom 1 cm and top 20% to 35% of the water column, the calculated total longshore transport rate may carry considerable uncertainty of up to 30% to 40%. Uncertainties associated with the estimate of local longshore sediment flux, especially the small values in the mid-surf zone, can be as high as 200%. Based on a simultaneous field measurement of longshore current and sediment concentration, Beach and Sternberg (1992) concluded that the product of time-averaged longshore current and concentration yields a reasonable estimate of longshore sediment flux at the measurement point.

The longshore flux was also calculated as the product of depth- and time-averaged current and the mean concentration over the measured portion of the water column, and compared with the measured values at traps from 2.7 to 11.6 m from shoreline. This calculation (denoted as "depth-averaged calculation" in Fig. 25) yielded greater sediment fluxes than computed from integration of the sediment-flux profile. For the spilling case, sediment flux obtained from the depth-averaging calculation was significantly greater than the flux measured at the downdrift bottom traps. For the plunging case, the depth-averaging calculation resulted in considerable overprediction in the vicinity of the breaker line, while the match in the mid-surf zone was reasonable. Because sediment concentration decreases much more rapidly away from the bed than the increase of longshore current at most of the cross-shore locations, and the neglect of the top 20% to 35% of water column, the product of depth-averaged velocity (approximately equal to 1/3-depth velocity) and concentration (approximately equal to 1/5-depth concentration) will almost always result in greater total flux than that derived from a more accurate integration of the sediment-flux profile. The total longshore transport rate across the section obtained from the depth-averaged fluxes were 4400 m^3/year for the spilling case and 4500 m^3/year for the plunging case, compared to the measured rates of 1200 m^3/year for the spilling and 3600 m^3/year for the plunging case. The closer match for the plunging case is likely to be a coincidence.

The total rates of longshore sediment transport measured at the downdrift traps were substantially different for the spilling and the plunging cases, 1200 vs. 3600 m^3/year for the section of beach from 2.7 to 11.6 m from the shoreline. The rate for the spilling case was 33% of the plunging-case rate although the breaker height and breaker angle were similar (Table 2). Wang et al. (2002) discussed in detail the differences between the total transport rates across the entire surf zone for the two cases.

4.5.2. Cross-shore sediment flux

Similar time-shifted calculations of instantaneous sediment flux, as described above, were conducted in the cross-shore direction. Cross-shore flux is much more significantly influenced by individual wave motions than longshore flux. Large variations of over 100% were obtained when comparing the flux obtained from the product of time-averaged cross-shore current and time-averaged sediment concentration with the time averages of the shifted instantaneous flux for both spilling (Fig. 26, upper panel) and plunging (Fig. 26, lower panel) cases. Compared to longshore flux, the variations in the cross-shore flux were much greater. Although it is not clear which of the shifted values represents the true flux, and it is possible that the product of time-averaged velocity and concentration may coincide with the true flux, this occurrence is neither likely nor reliable given the large and variable differences.

The present experiments were conducted after a series of preexperiment runs that were designed to establish optimal pump settings to circulate the wave-generated longshore current (Hamilton and Ebersole, 2001) and to allow the beach profile to reach an equilibrium shape. Because the beach reached quasi-

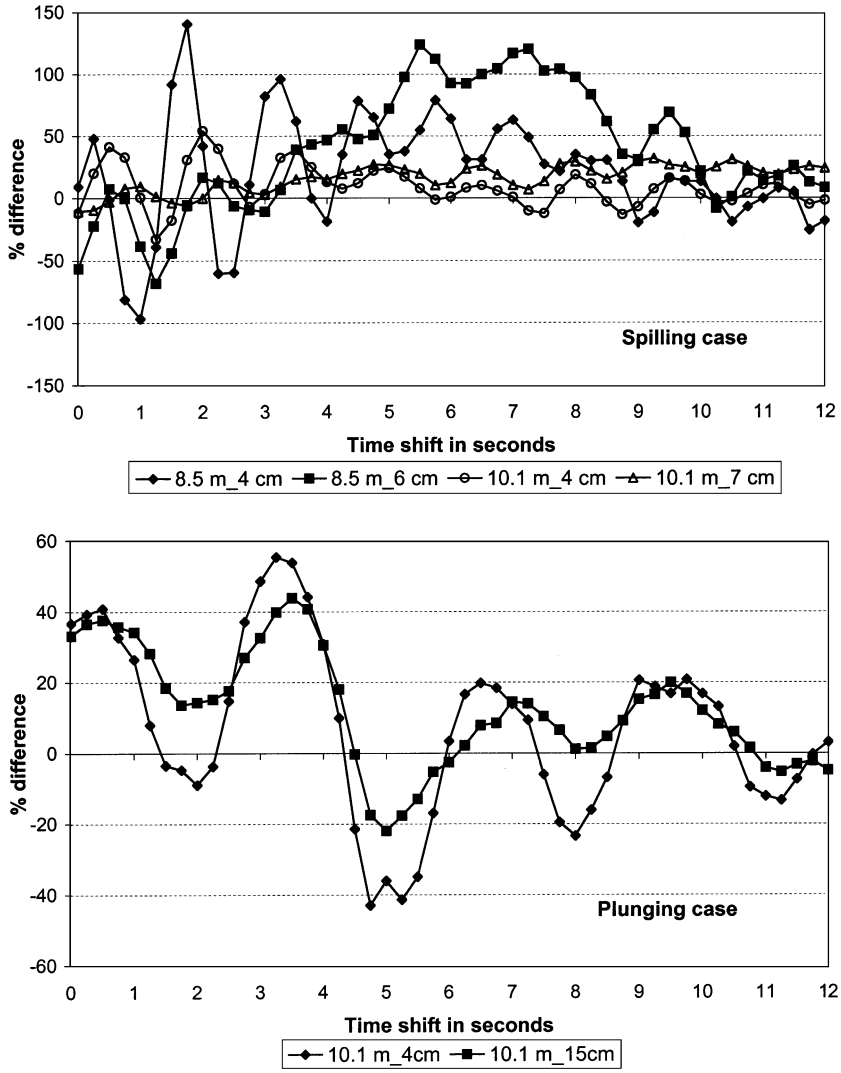

Fig. 26. Time averages of the "shifted" cross-shore flux in comparison with flux obtained from the product of time-averaged cross-shore current and time-averaged concentration. Legends refer to distance from the shoreline and sensor elevation.

equilibrium condition during the experiments, net cross-shore sediment flux should be close to zero along most of the profile. No appreciable gradients in longshore current and sediment concentration, and therefore in longshore sediment flux, were measured over the middle section of the test beach. This uniform longshore transport regime should not cause any morphological changes and surveys confirmed that this was the case. The product of time-averaged velocity and time-averaged concentration, however, indicates that the net sediment transport is directed offshore due to the near-bed seaward-directed flow and the large near-bed sediment concentration. The calculated offshore sediment flux is substantial and conflicts with the stable beach profile. This, together with the great temporal variations of both cross-shore current and sediment concentration, leads to the conclusion that cross-shore sediment flux cannot be estimated accurately via the product of time-averaged velocity and time-averaged sediment concentration.

Osborne and Greenwood (1992) performed a detailed field study of sand transport across a barred coast. They found that all three, i.e., average, high-, and low-frequency components (Eqs. (2)–(5)), were important in contributing to cross-shore flux, and a different term tends to dominate at different cross-shore locations. Generally, the time-averaged terms (first term on the right-hand side of Eq. (5)) have significant influence on offshore-directed transport. For onshore-directed transport, the frequency-dependent terms (second and third terms in Eq. (5)) play significant and complicated roles. Van Rijn and Havinga (1995) and Grasmeijer and Van Rijn (1999) found similar results from a series of laboratory studies.

5. Concluding summary

In general, surf-zone currents and sediment concentrations are characterized by rapid and substantial temporal and spatial variations. Patterns of temporal and spatial variations of longshore current, cross-shore current, and sediment concentration are significantly different. Caution should be exercised when averaging these parameters over time and space and using the averaged values to calculate mean sediment flux.

Compared to the magnitude of temporal variations of cross-shore current and sediment concentration, longshore current remained relatively steady over time and did not seem to be influenced significantly by individual wave motions for the present small breaker angle of 6.5°. The vertical structure of time-averaged longshore current exhibited a logarithmic upward increasing trend, as opposed to a general comprehension of homogeneous longshore current profiles. The time- and depth-averaged longshore current, not counting the portion of the water column above the wave trough, matched well with the time-averaged current measured at an elevation from the bed equal to 1/3 still-water depth. For the two irregular wave cases characterized by different breaker types, the cross-shore distribution of depth-averaged longshore current remained relatively uniform over much of the mid-surf zone, with a minor peak measured just seaward of the swash zone and a decreasing trend through the incipient breaker zone.

Cross-shore current varies greatly and rapidly with time, dominated by individual wave motions. The vertical structure of the time-averaged cross-shore current demonstrates the commonly observed structure of undertow, with onshore flow in the upper water column and offshore flow in the lower water column, divided at the level of the wave trough. The shape of the mean cross-shore current profile can be reasonably approximated with parabolic curves although the goodness-of-fit was better for the spilling than the plunging case.

Sediment concentration decreases rapidly, over nearly four orders of magnitude, upward through the water column across most of the surf zone. An exception occurred at the breaker line for the plunging case, where relatively homogeneous concentration was measured throughout the water column above 4 cm from the bed. Temporal variations of sediment suspension were dominated by events of large concentration. Qualitatively, the sediment-suspension events were controlled by local patterns of wave breaking. This is observed at the plunging breaker line, where local sediment-suspension events are strongly influenced by the location of the plunging point. The point of plunging varied considerably for the irregular wave cases. Temporal variations at different elevations in the water column were not exactly in phase although a similar general trend was observed at times, indicating that horizontal advection may not be neglected at small temporal scales.

Nearly identical sediment concentrations were measured within 3 cm from the bed near the breaker line for both the spilling and the plunging cases, despite the significant differences in bed conditions, near-bottom velocities, and turbulence intensities. While high in the water column, approximately one order of magnitude greater sediment concentration was measured at the plunging breaker line than at the spilling breaker line. Across most of the surf-bore-dominated mid-surf zone, suspended sediment concentrations were rather similar for both the plunging and the spilling cases.

The product of time-averaged profiles of longshore current and sediment concentration, and their integration over depth, yields a reasonable estimate of longshore sediment flux, as compared to the measured amount at the downdrift traps. This is attributable to the relatively steady longshore current and possibly to the cancellation of the time-varying contributions during averaging. Uncertainties of up to 30% to

40% may be associated with the above computation of longshore transport rate. Estimates of local flux, especially the small values in the mid-surf zone, may involve up to 200% uncertainty. The accuracies of the estimations may be improved if the transport in the bottom 1 cm and in the top 20% to 35% of water column is included. Net cross-shore sediment flux obtained from the product of time-averaged current and sediment concentration did not agree with the overall trend of beach-profile change.

At the breaker line for the plunging case, longshore sediment flux is dominated by sediment transport above 5 cm from the bed. Less than 30% of the sediment transport occurred within the lowermost 5 cm or the lower 20%, of the water column. While across most of the rest of the surf zone, over 70% of the total longshore flux occurred within 5 cm from the bed. For the spilling case across the entire surf zone, near-bed sediment transport dominated, with over 70% of the total flux occurring within 5 cm of the bed.

The longshore sediment transport rate measured across the entire surf zone for the plunging case was substantially greater than that measured for the spilling case although the breaker height and breaker angle were similar for the two cases. Breaker type has significant influence on the rate of longshore sediment transport.

Acknowledgements

William Halford, David Daily, and Tim Nisley provided technical support for this study. We thank Carl Miller and Reggie Beach for providing the FOBS sensors. The paper has benefited greatly from the constructive reviews by Drs. Robert Dean and J. van de Graaff. Ping Wang is jointly funded by the U.S. Army Engineer Research and Development Center and the Louisiana Sea Grant College Program. Permission to publish this paper was granted by the Headquarters, U.S. Army Corps of Engineers.

References

Beach, R.A., Sternberg, R.W., 1992. Suspended sediment transport in the surf zone: response to incident wave and longshore current interaction. Marine Geology 108, 275–294.

Beach, R.A., Sternberg, R.W., Johnson, R., 1992. A fiber optic sensor for monitoring suspended sediment. Marine Geology 103, 513–520.

Bosman, J., 1982. Concentration measurements under oscillatory motion. Delft Hydraulics, Report MI695-II, Delft, The Netherlands.

Bouws, E.H., Rosenthal, G.W., Vincent, C.L., 1985. Similarity of the wind wave spectra in finite water depth: 1. Spectral form. Journal of Geophysical Research 90, 975–986.

Bruun, P., 1954. Coast erosion and the development of beach profiles. Technical Memorandum No. 44, Beach Erosion Board.

Dean, R.G., 1977. Equilibrium beach profiles: U.S. Atlantic and Gulf coasts. Ocean Engineering Report No. 12, Department of Civil Engineering, University of Delaware, Newark, DE.

Dean, R.G., 1991. Equilibrium beach profiles: characteristics and applications. Journal of Coastal Research 7, 53–84.

Dean, R.G., Zheng, J., 1994. Cross-shore sediment transport relationships. UFL/COEL-94/018. Coastal and Oceanographic Engineering Department, University of Florida, Gainesville, FL, 33 pp.

Garcez Faria, A.F., Thornton, E.B., Lippmann, T.C., Stanton, T.P., 2000. Undertow over a barred beach. Journal of Geophysical Research 105, 16999–17010.

Grasmeijer, B.T., Van Rijn, L.C., 1999. Transport of fine sand by currents and waves: III. Breaking waves over a barred profile with ripples. Journal of Waterways, Port, Coastal, and Ocean Engineering, ASCE 125, 71–79.

Guza, R.T., Thornton, E.B., 1982. Swash oscillations on a natural beach. Journal of Geophysical Research 87, 483–491.

Hallermeier, R.J., 1981. Terminal settling velocity of commonly occurring sand grains. Sedimentology 28, 859–865.

Hamilton, D.G., Ebersole, B.A., 2001. Establishing uniform longshore currents in a large-scale laboratory facility. Coastal Engineering, 199–218.

Hamilton, D.G., Ebersole, B.A., Smith, E.R., Wang, P., 2001. Development of a large-scale laboratory facility for sediment transport research. Technical Report, ERDC/CHL TR-01-22, U.S. Army Engineer Waterways Experiment Station, Vicksburg, MS.

Huntley, D.A., Guza, R.T., Thornton, E.B., 1981. Field observations of surf beat: 1. Progressive edge waves. Journal of Geophysical Research 83, 1913–1920.

Johnson, B.D., Kobayashi, N., 2000. Free surface statistics and probabilities in the surf zone on beaches. Proceedings of 27th International Conference on Coastal Engineering. ASCE Press, New York, pp. 1022–1035.

Kana, T.W., 1979. Suspended sediment in breaking waves. Technical Report No. 18-CRD, University of South Carolina, Department of Geology, Columbia, SC, 153 pp.

Kraus, N.C., 1987. Application of portable traps for obtaining point measurement of sediment transport rates in the surf zone. Journal of Coastal Research 2, 139–152.

Kraus, N.C., Dean, J.L., 1987. Longshore sediment transport rate distribution measured by trap. Proceedings of Coastal Sediment'87. ASCE Press, New York, pp. 881–896.

Kraus, N.C., Sasaki, T.O., 1979. Influence of wave angle and lateral mixing on the longshore current. Marine Science Communications 5 (2), 91–126.

Kraus, N.C., Gingerich, K.J., Rosati, J.D., 1988. Toward an improved empirical formula for longshore sand transport. Proceedings of 21st International Conference on Coastal Engineering. ASCE Press, New York, pp. 1183–1196.

Kraus, N.C., Lohrmann, A., Cabrera, R., 1994. New acoustic meter for measuring 3D laboratory flows. Journal of Hydraulic Engineering 120 (3), 406–412.

Longuet-Higgins, M.S., 1970. Longshore currents generated by obliquely incident sea waves, 1 and 2. Journal of Geophysical Research 75, 6778–6810.

Miller, H.C., 1998. Comparison of storm longshore transport rates to predictions. Proceedings of 26th International Conference on Coastal Engineering. ASCE Press, New York, pp. 2953–2967.

Miller, H.C., 1999. Field measurements of longshore sediment transport during storms. Coastal Engineering 36, 301–321.

Nielsen, P., 1979. Some basic concepts of wave sediment transport. Serial Paper 20, Institute of Hydrodynamic and Hydraulic Engineering, Technical University of Denmark, 160 pp.

Nielsen, P., 1992. Coastal Bottom Boundary Layers and Sediment Transport. World Scientific, Singapore, 324 pp.

Osborne, P.D., Greenwood, B.G., 1992. Frequency-dependent cross-shore suspended sediment transport: 2. A barred shoreface. Marine Geology 106, 25–51.

Osborne, P.O., Greenwood, B., 1993. Sediment suspension under waves and currents: time scales and vertical structures. Sedimentology 40, 599–622.

Puelo, J.A., Beach, R.A., Holman, R.A., Allen, J.S., 2000. Swash zone sediment suspension and transport and the importance of bore-generated turbulence. Journal of Geophysical Research 105, 17021–17043.

Rattanapitikon, W., Shibayama, T., 2000. Simple model for undertow profile. Coastal Engineering Journal, JSCE 42, 1–30.

Smith, J.M., Larson, M., Kraus, N.C., 1993. Longshore current on a barred beach: field measurements and calculations. Journal of Geophysical Research 98, 22717–22731.

Svendsen, I.A., 1984. Mass flux and undertow in a surf zone. Coastal Engineering 8, 303–330.

Svendsen, I.A., Lorenz, R.S., 1989. Velocities in combined undertow and longshore currents. Coastal Engineering 13, 55–79.

Thompson, E.F., Briggs, M.J., 1993. Surf Beat in Coastal Waters. Technical Report CERC-93-12, U.S. Army Corps of Engineers Waterways Experiment Station, Vicksburg, MS.

Thornton, E.B., Guza, R.T., 1986. Surf zone longshore currents and random waves: field data and models. Journal of Physical Oceanography 16, 1165–1178.

Thornton, E.B., Humiston, R.T., Birkemeier, W., 1996. Bar/trough generation on a natural beach. Journal of Geophysical Research 101, 12097–12110.

U.S. Army Corps of Engineers (USACE), 1984. Shore Protection Manual. Waterways Experiment Station, Coastal Engineering Research Center, U.S. Government Printing Office, Washington, DC.

Van Rijn, L.C., 1993. Principles of Sediment Transport in Rivers, Estuaries and Coastal Seas. Aqua Publications, The Netherlands.

Van Rijn, L.C., Havinga, F.J., 1995. Transport of fine sands by currents and waves: II. Journal of Waterways, Port, Coastal, and Ocean Engineering, ASCE 121, 123–133.

Visser, P.J., 1991. Laboratory measurements of uniform longshore current. Coastal Engineering 15, 563–593.

Wang, P., 1998. Longshore sediment flux in water column and across surf zone. Journal of Waterway Port, Coastal, and Ocean Engineering, ASCE 124 (3), 108–117.

Wang, P., Kraus, N.C., 2002. Movable bed model investigation of groin notching. Journal of Coastal Research, Special Issue, in press.

Wang, P., Kraus, N.C., Davis Jr., R.A., 1998. Total longshore sediment transport rate in the surf zone: field measurements and empirical predictions. Journal of Coastal Research 14 (1), 269–282.

Wang, P., Smith, E.R, Ebersole, B.A., 2002. Large-scale laboratory measurements of longshore sediment transport under spilling and plunging breakers. Journal of Coastal Research 18 (1), 118–135.

Welch, P.D., 1967. The use of fast Fourier transformation for the estimation of power spectra: a method based on time averaging over short, modified periodograms. IEEE Transactions on Audio and Electracoustics AU-15, 70–73.

Wikramanayake, P.N., Madsen, O.S., 1994a. Calculation of suspended sediment transport by combined wave-current flows. Contract Report DRP-94-7, U.S. Army Engineer Waterways Experiment Station, Vicksburg, MS, 148 pp.

Wikramanayake, P.N., Madsen, O.S., 1994b. Calculation of movable bed friction factors. Contract Report DRP-94-5, U.S. Army Engineer Waterways Experiment Station, Vicksburg, MS, 152 pp.

Zampol, J.A., Inman, D.L., 1989. Discrete measurement of suspended sediment. In: Seymour, R.J. (Ed.), Nearshore Sediment Transport. Plenum, New York, pp. 257–285.

Zheng, J., Dean, R.G., 1997. Numerical models and intercomparisons of beach profile evolution. Coastal Engineering 30, 169–201.